University of Wollongong

Research Online

Faculty of Science, Medicine and Health - Papers: Part B

Faculty of Science, Medicine and Health

1-1-2019

Role of RNase H enzymes in maintaining genome stability in Escherichia coli expressing a steric-gate mutant of pol VICE391

Erin Walsh
National Institute of Child Health and Human Development

Sarah Henrikus
University of Wollongong, ssh997@uowmail.edu.au

Alexandra Vaisman
National Institute of Child Health and Human Development

Karolina Makiela-Dzbenska
Polish Academy of Sciences

Thomas Armstrong
University of Wollongong, tja069@uowmail.edu.au

See next page for additional authors

Follow this and additional works at: https://ro.uow.edu.au/smhpapers1

Publication Details Citation

Walsh, E., Henrikus, S., Vaisman, A., Makiela-Dzbenska, K., Armstrong, T., Lazowski, K., Mcdonald, J. P., Goodman, M. F., van Oijen, A. M., Jonczyk, P., Fijalkowska, I., Robinson, A., & Woodgate, R. (2019). Role of RNase H enzymes in maintaining genome stability in Escherichia coli expressing a steric-gate mutant of pol VICE391. Faculty of Science, Medicine and Health - Papers: Part B. Retrieved from https://ro.uow.edu.au/smhpapers1/1047

Research Online is the open access institutional repository for the University of Wollongong. For further information contact the UOW Library: research-pubs@uow.edu.au

Role of RNase H enzymes in maintaining genome stability in Escherichia coli expressing a steric-gate mutant of pol VICE391

Abstract

pol VICE391 (RumA′2B) is a low-fidelity polymerase that promotes considerably higher levels of spontaneous "SOS-induced" mutagenesis than the related E. coli pol V (UmuD′2C). The molecular basis for the enhanced mutagenesis was previously unknown. Using single molecule fluorescence microscopy to visualize pol V enzymes, we discovered that the elevated levels of mutagenesis are likely due, in part, to prolonged binding of RumB to genomic DNA leading to increased levels of DNA synthesis compared to UmuC. We have generated a steric gate pol VICE391 variant (pol VICE391_Y13A) that readily misincorporates ribonucleotides into the E. coli genome and have used the enzyme to investigate the molecular mechanisms of Ribonucleotide Excision Repair (RER) under conditions of increased ribonucleotide-induced stress. To do so, we compared the extent of spontaneous mutagenesis promoted by pol V and pol VICE391 to that of their respective steric gate variants. Levels of mutagenesis promoted by the steric gate variants that are lower than that of the wild-type enzyme are indicative of active RER that removes misincorporated ribonucleotides, but also misincorporated deoxyribonucleotides from the genome. Using such an approach, we confirmed that RNase HII plays a pivotal role in RER. In the absence of RNase HII, Nucleotide Excision Repair (NER) proteins help remove misincorporated ribonucleotides. However, significant RER occurs in the absence of RNase HII and NER. Most of the RNase HII and NER-independent RER occurs on the lagging strand during genome duplication. We suggest that this is most likely due to efficient RNase HI-dependent RER which recognizes the polyribonucleotide tracts generated by pol VICE391_Y13A. These activities are critical for the maintenance of genomic integrity when RNase HII is overwhelmed, or inactivated, as ΔrnhB or ΔrnhB ΔuvrA strains expressing pol VICE391_Y13A exhibit genome and plasmid instability in the absence of RNase HI.

Publication Details

Walsh, E., Henrikus, S. S., Vaisman, A., Makiela-Dzbenska, K., Armstrong, T. J., Lazowski, K., McDonald, J. P., Goodman, M. F., van Oijen, A. M., Jonczyk, P., Fijalkowska, I. J., Robinson, A. & Woodgate, R. (2019). Role of RNase H enzymes in maintaining genome stability in Escherichia coli expressing a steric-gate mutant of pol VICE391. DNA Repair, 84 102685-1-102685-15.

Authors

Erin Walsh, Sarah Henrikus, Alexandra Vaisman, Karolina Makiela-Dzbenska, Thomas Armstrong, Krystian Lazowski, John P. Mcdonald, Myron F. Goodman, Antoine M. van Oijen, Piotr Jonczyk, Iwona Fijalkowska, Andrew Robinson, and Roger Woodgate

This journal article is available at Research Online: https://ro.uow.edu.au/smhpapers1/1047

DNA Repair 84 (2019) 102685

Contents lists available at ScienceDirect

DNA Repair

journal homepage: www.elsevier.com/locate/dnarepair

Role of RNase H enzymes in maintaining genome stability in *Escherichia coli* expressing a steric-gate mutant of pol V_{ICE391} ☆,☆☆

Erin Walsh[a], Sarah S. Henrikus[b,c], Alexandra Vaisman[a], Karolina Makiela-Dzbenska[d], Thomas J. Armstrong[b,c], Krystian Łazowski[d], John P. McDonald[a], Myron F. Goodman[e], Antoine M. van Oijen[b,c], Piotr Jonczyk[d], Iwona J. Fijalkowska[d], Andrew Robinson[b,c], Roger Woodgate[a,*]

[a] Laboratory of Genomic Integrity, National Institute of Child Health and Human Development, National Institutes of Health, Bethesda, MD 20892-3371, USA
[b] Molecular Horizons Institute and School of Chemistry and Biomolecular Science, University of Wollongong, Australia
[c] Illawarra Health and Medical Research Institute, Wollongong, Australia
[d] Institute of Biochemistry and Biophysics, Polish Academy of Sciences, Warsaw, Poland
[e] Departments of Biological Sciences and Chemistry, University of Southern California, Los Angeles, CA 90089-2910 USA

ARTICLE INFO

Keywords:
DNA polymerase V
Y-family DNA polymerase
Ribonucleotide excision repair
Translation

ABSTRACT

pol V_{ICE391} (RumA′$_2$B) is a low-fidelity polymerase that promotes considerably higher levels of spontaneous "SOS-induced" mutagenesis than the related *E. coli* pol V (UmuD′$_2$C). The molecular basis for the enhanced mutagenesis was previously unknown. Using single molecule fluorescence microscopy to visualize pol V enzymes, we discovered that the elevated levels of mutagenesis are likely due, in part, to prolonged binding of RumB to genomic DNA leading to increased levels of DNA synthesis compared to UmuC.

We have generated a steric gate pol V_{ICE391} variant (pol V_{ICE391}_Y13A) that readily misincorporates ribonucleotides into the *E. coli* genome and have used the enzyme to investigate the molecular mechanisms of Ribonucleotide Excision Repair (RER) under conditions of increased ribonucleotide-induced stress. To do so, we compared the extent of spontaneous mutagenesis promoted by pol V and pol V_{ICE391} to that of their respective steric gate variants. Levels of mutagenesis promoted by the steric gate variants that are lower than that of the wild-type enzyme are indicative of active RER that removes misincorporated ribonucleotides, but also misincorporated deoxyribonucleotides from the genome.

Using such an approach, we confirmed that RNase HII plays a pivotal role in RER. In the absence of RNase HII, Nucleotide Excision Repair (NER) proteins help remove misincorporated ribonucleotides. However, significant RER occurs in the absence of RNase HII and NER. Most of the RNase HII and NER-independent RER occurs on the lagging strand during genome duplication. We suggest that this is most likely due to efficient RNase HI-dependent RER which recognizes the polyribonucleotide tracts generated by pol V_{ICE391}_Y13A. These activities are critical for the maintenance of genomic integrity when RNase HII is overwhelmed, or inactivated, as Δ*rnhB* or Δ*rnhB* Δ*uvrA* strains expressing pol V_{ICE391}_Y13A exhibit genome and plasmid instability in the absence of RNase HI.

1. Introduction

Escherichia coli DNA polymerase V (pol V), a trimeric UmuD′$_2$C complex [1], is a Y-family polymerase [2] that is best characterized for its ability to promote damage-induced "SOS"-mutagenesis [3,4]. The mutagenesis occurs during error-prone translesion synthesis (TLS) across lesions that would otherwise block the cell's replicase, DNA polymerase III (pol III) [5,6]. Because of its error-prone DNA synthesis, pol V is subject to multiple levels of regulation [7]. This includes LexA-regulated transcriptional control; activated RecA*-mediated post-translational modification; Lon- and ClpXP- targeted proteolysis; the need for additional specific protein-protein interactions; as well as spatial regulation

Abbreviations: DNA, polymerase pol; TLS, translesion DNA synthesis; RER, ribonucleotide excision repair; NER, nucleotide excision repair

☆ This Special Issue is edited by Robert Crouch, Guest Editor.

☆☆ This article is part of the special issue "RNases H".

* Corresponding author at: 9800 Medical Center Drive, Building C, Rm 320, Bethesda, MD 20892-3371, USA.
E-mail address: woodgate@nih.gov (R. Woodgate).

https://doi.org/10.1016/j.dnarep.2019.102685
Received 8 March 2019; Received in revised form 31 July 2019; Accepted 3 August 2019
Available online 10 August 2019
1568-7864/ Published by Elsevier B.V. This is an open access article under the CC BY-NC-ND license (http://creativecommons.org/licenses/BY-NC-ND/4.0/).

inside the cell. As a result, pol V activity is usually kept to a minimum, such that it is utilized only when absolutely required.

However, in a *lexA*(Def) *recA730* genetic background, in which the RecA730 (E38 K) protein is in a constitutively activated state (RecA*), virtually all of the regulation normally imposed on pol V activity in a wild-type cell is circumvented, allowing error-prone pol V to replicate undamaged DNA. This leads to a roughly 100-fold increase in so-called "SOS-dependent spontaneous mutagenesis" [8]. It is believed that this mutagenesis occurs, in part, due to the higher basal steady state levels of pol V in undamaged *recA730* strains compared to *recA*$^+$ strains (~20 pol V molecules in a *recA730* cell *vs*. one pol V molecule in a *recA*$^+$ cell [9]) that transiently compete with pol III for access to undamaged DNA [10]. Studies with *lacZ* reporter alleles suggest that this occurs primarily on the lagging strand during genome duplication [11].

The intracellular levels of ribonucleotides in a cell are considerably higher (up to 1000-fold) than the concentrations of the corresponding deoxyribonucleotides [12–14]. It is now well established that the main line of defense against errant misincorporation of ribonucleotides by DNA polymerases is a so-called "steric gate", which usually comprises a single amino acid residue with a bulky side chain that physically clashes with the 2′-OH of the incoming ribonucleotide to prevent its misincorporation into DNA [15–17]. Mutant DNA polymerases in which the bulky side chain of the steric gate amino acid has been replaced with a much smaller moiety have been widely used to increase the levels of

Table 1
E. coli strains used in this study.

Strain	Relevant Genotype	Source or Reference
MG1655	F- λ- *rph-*	*E. coli* Genetic Stock Center
JJC5945	F- λ- *rph- dnaX-YPet*::Kan	Benedict Michel, [67]
BW7261	*Hfr(PO2A) leu-63*::*Tn10 fhuA22 Δ(argF-lac)169 ompF627 relA1 spoT1*	*E. coli* Genetic Stock Center
RW82	*Δ(umuDC)595*::*cat*	[68]
RW880	F- λ$^-$ *rph- Δ(umuDC)595*::*cat*	MG1655 x P1.RW82
SSH037	F- λ$^-$ *rph- dnaX-YPet*::Kan *Δ(umuDC)595*::*cat*	JJC5945 x P1.RW880
SSH073	as SSH037, but harboring pJM1337	This work
SSH074	as SSH037, but harboring pJM1350	This work
EAW287	F- λ$^-$ *rph- recA730 sulA*$^-$	[9]
SSH116	F- λ$^-$ *rph- recA730 sulA*$^-$ *dnaX-YPet*	EAW287 x P1.AR164
SSH117	F- λ$^-$ *rph- recA730 sulA*$^-$ *dnaX-YPet Δ(umuDC)595*::*cat*	SSH116 x P1.RW880
SSH118	as SSH117, but harboring pJM1324	This work
SSH119	as SSH117, but harboring pJM1334	This work
RW584[a]	*recA730 lexA51*(Def) *Δ(umuDC)596*::*ermGT*	[69]
RW1448[b,c]	*recA730 lexA51*(Def) *Δ(umuDC)596*::*ermGT ΔdinB61*::*ble*	RW698 x BW7261
NR9566	*dnaE915 yafC502*::Tn*10*	Roel Schaaper, [70]
RW1560[b]	*recA730 lexA51*(Def) *Δ(umuDC)596*::*ermGT ΔdinB61*::*ble dnaE915 yafC502*::Tn*10*	RW1448 x P1.NR9566
RW698[a]	*recA730 lexA51*(Def) *Δ(umuDC)596*::*ermGT*	[25]
RW970[a]	*recA730 lexA51*(Def) *Δ(umuDC)596*::*ermGT ΔdinB61*::*ble ΔrnhB782*	[25]
RW902[a]	*recA730 lexA51*(Def) *Δ(umuDC)596*::*ermGT ΔdinB61*::*ble ΔuvrA753*::Kan	[25]
RW1044[a]	*recA730 lexA51*(Def) *Δ(umuDC)596*::*ermGT ΔdinB61*::*ble ΔrnhA319*::*cat*	[25]
RW1092[a]	*recA730 lexA51*(Def) *Δ(umuDC)596*::*ermGT ΔdinB61*::*ble ΔrnhB782 ΔrnhA319*::*cat*	[25]
RW990[a]	*recA730 lexA51*(Def) *Δ(umuDC)596*::*ermGT ΔdinB61*::*ble ΔrnhB782 ΔuvrA753*::Kan	[26]
RW1190[a]	*recA730 lexA51*(Def) *Δ(umuDC)596*::*ermGT ΔdinB61*::*ble ΔrnhB782 ΔrnhA319*::*cat ΔuvrA753*::Kan	[26]
RW1450[b,c]	*recA730 lexA51*(Def) *Δ(umuDC)596*::*ermGT ΔdinB61*::ble *ΔrnhB782*	RW970 x BW7261
EC9998[b,c]	*recA730 lexA51*(Def) *Δ(umuDC)596*::*ermGT ΔdinB61*::*ble ΔuvrA753*::Kan	RW902 x BW7261
RW1510[b,c]	*recA730 lexA51*(Def) *Δ(umuDC)596*::*ermGT ΔdinB61*::*ble ΔrnhB782 ΔuvrA753*::Kan	RW990 x BW7261

[a] Full genotype: *thr-1 araD139 Δ(gpt-proA)62 lacY1 tsx-33 glnV44 galK2 hisG4 rpsL31 xyl-5 mtl-1 argE3 thi-1 sulA211 lexA51*(Def) *recA730 Δ(umuDC)596*::*ermGT ΔdinB61*::*ble*.

[b] As "a", but *gpt*$^+$ *proA*$^+$ *Δ(argF-lac)169*.

[c] For the *lacZ* reversion assay, the above strains[b] were used to construct pairs of *lacZ* derivatives, as described in [33]. These strains carry a chromosomal copy of the *lacZ* missense allele from strain CC105 [32], in one of the two orientations, with respect to the origin of replication (Left or Right).

errant ribonucleotides misincorporated into DNA and to elucidate the mechanism of their subsequent removal during Ribonucleotide Excision Repair (RER) [18–23]. Indeed, we previously utilized a steric gate pol V mutant with a Y11A substitution in the catalytic UmuC subunit of the polymerase to investigate the mechanisms of RER in *E. coli* [24,25]. *In vitro* studies with the pol V_Y11A mutant revealed that the enzyme not only distinguishes poorly between ribo- and deoxyribonucleotides, but also exhibits low base selectivity [24]. We therefore expected the pol V_Y11A mutant to promote high levels of SOS-dependent mutagenesis *in vivo*. To our surprise, the level of mutagenesis was a fraction of that promoted by wild-type pol V [24]. To explain these observations, we hypothesized that misincorporated deoxyribonucleotides were removed by active RER triggered by the misincorporated ribonucleotides. We further hypothesized that if all RER pathways were inactivated, pol V_Y11A-dependent mutagenesis would be as high as (or even higher than) that promoted by wild-type pol V [26]. On the basis of these hypotheses, we discovered that RNase HII encoded by *rnhB*, provides the lead role in RER in *E. coli*, while RNase HI (encoded by *rnhA*) and the Nucleotide Excision Repair proteins (encoded by *uvrA*, *uvrB* and *uvrC*) provide back-up roles in the absence of RNase HII [26].

Although *E. coli* pol V promotes significant levels of SOS-dependent spontaneous mutagenesis, orthologs of pol V, such as polR1 (comprising MucA′$_2$B and encoded by *mucAB* on R46/pKM101, and used to increase the efficacy of mutagen detection in the "Ames-test") [27], or pol V$_{ICE391}$ (comprising RumA′$_2$B and encoded by *rumAB* on R391/ICE391) [28,29] are much more efficient at promoting SOS-dependent spontaneous mutagenesis [30]. Indeed, pol V$_{ICE391}$ is the most potent pol V mutator reported in the literature to date [30].

We were therefore interested in recapitulating our earlier RER studies with the *E. coli* pol V_Y11A using a steric gate mutant of pol V$_{ICE391}$ harboring a Y13A substitution in its catalytic RumB subunit. Our initial studies suggest that pol V$_{ICE391}$ can bind to undamaged DNA more frequently, and for far longer, than *E. coli* pol V. Our expectation was that the more potent pol V$_{ICE391}$_Y13A enzyme would potentially increase the number of errantly misincorporated ribonucleotides into the *E. coli* genome and possibly reveal additional pathways of RER. Our studies suggest that while RNase HII maintains its pivotal role in RER, the increased load of ribonucleotides incorporated into the genome by pol V$_{ICE391}$_Y13A leads to a greater dependency on RNase HI to protect *E. coli* from the deleterious effects of errant ribonucleotide incorporation into its genome.

2. Materials and methods

2.1. Bacterial strains and plasmids

Bacterial strains used in this study are described in Table 1. New strains were generated *via* generalized transduction using P1*vir* [31]. Where noted, the following antibiotics were used for selection; zeocin (25 μg/ml), kanamycin (50 μg/ml), tetracycline (15 μg/ml), chloramphenicol (20 μg/ml), ampicillin (100 μg/ml) and spectinomycin (50 μg/ml).

The *E. coli* strains used for the leading/lagging strand mutagenesis assay (see section 2.5 below) are derivatives of RW698 [26], but carry a *lacZ* missense allele that allows for scoring of mutagenesis *via* reversion to Lac$^+$ by an A·T→T·A transversion [32], inserted into the phage λ attachment site in one of the two orientations (Left and Right) with respect to the origin of replication [33]. Recipient pairs of *lacZ* integrants were transformed with low-copy-number plasmids expressing either wild-type pol V$_{ICE391}$ (pRW320), the pol V$_{ICE391}$_Y13A variant (pJM1282), or the control vector (pGB2), to measure mutagenesis levels on the leading and lagging DNA strands.

Plasmids used in this study are described in Table 2. A low-copy-number plasmid, pJM1282, expressing a Y13A steric gate variant of *rumB* was generated by synthesizing a *Bam*HI to *Acc*I fragment (Genscript) containing the Y13A allele marked with a *Bss*HII site into the corresponding sites of pRW320 [34]. The mKate2-RumB containing plasmid, pJM1324, was constructed by sub-cloning an N-terminal mKate2-RumB chimera (Genscript) into pRW320 from *Ale*I to *Pml*I. Subsequently, a fragment carrying the catalytically inactive D103A-E104A double mutation in *rumB* (Genscript) was sub-cloned into pJM1324 from *Pml*I to *Acc*I to generate pJM1347. In addition, a fragment carrying the β-clamp binding site mutant, Q358A-L361A-F364A in *rumB* (Genscript) was sub-cloned into pJM1324 from *Msc*I to *Nar*I to generate pJM1350. A C-terminal *umuC-mKate2* chimera was generated by synthesizing a *Bam*HI fragment containing the desired gene fusion and sub-cloned into the unique *Bam*HI site of pRW134 [34]. One clone with *umuC-mKate2* in the correct orientation was designated as pJM1334.

pJM1295, which expresses N-terminal His-tagged RumB_Y13A was generated by cloning a synthesized *Xba*I-*Nco*I *rumB* fragment with the Y13A substitution (Genscript) into pHRB1 [35].

Table 2
E. coli plasmids used in this study.

Plasmid	Relevant Characteristics	Source or Reference
pGB2	Low-copy-number, Spc^R vector	[71]
pRW134	pGB2, *umuD′C*	[34]
pJM963	pGB2, *umuD′C*_Y11A [steric gate mutant]	[72]
pRW320	pGB2, *rumA′B*	[34]
pJM1282	pGB2, *rumA′B*_Y13A [steric gate mutant]	This work
pJM1324	pGB2, *rumA′ mKate2-rumB*	This work
pJM1334	pGB2, *umuD′ umuC-mKate2*	This work
pJM1347	pGB2, *rumA′ mKate2-rumB*_D103A-E104A [catalytically dead]	This work
pJM1350	pGB2, *rumA′ mKate2-rumB*_ Q358A-L361A-F364A [β-clamp mutant]	This work
pARA1	High copy, Amp^R, RumA′ expressed from the *Ara* promoter	[35]
pHRB1	pGB2, Kan^R, low expression of His-Tagged RumB	[35]
pJM1295	pHRB1, but expressing His-Tagged RumB_Y13A	This work

2.2. Quantitative spontaneous mutagenesis

E. coli cells were transformed with the one of the following plasmids and grown at 37 °C overnight in LB media containing spectinomycin: pGB2 (low-copy-number vector), or low-copy plasmids expressing pol V (pRW134), pol V_Y11A steric gate mutant (pJM963), pol V$_{ICE391}$ (pRW320), or pol V$_{ICE391}$_Y13A steric gate mutant (pJM1282). The following day, cells were isolated by centrifugation and resuspended in an equal volume of SM buffer [31]. To determine the number of spontaneously arising histidine revertant (His$^+$) mutants, (100 μl) cells were seeded upon Davis and Mingioli minimal agar plates [36] containing glucose (0.4% wt/vol); agar (1.0% wt/vol); proline, threonine, valine, leucine and isoleucine (all at 100 μg/ml); thiamine (0.25 μg/ml); and histidine (1 μg/ml). Spontaneously arising His$^+$ mutants were counted after four days growth at 37 °C and are a direct measure of the spontaneous mutagenesis frequency since the number of mutants that arise on each plate is dependent on the limiting amount of histidine present in the media, independent of the number of cells seeded.

2.3. Western blotting to detect plasmid encoded UmuC proteins

Overnight cultures of RW584 harboring pRW134 or pJM1334 were grown in LB media containing 50 μg/ml spectinomycin. The next day, the cultures were diluted 1:100 in fresh LB containing spectinomycin and grown to mid-log (~OD 0.5) (~3 h). Whole cell extracts were made by centrifuging 1.5 ml of culture and adding 90 μl of sterile deionized water and 30 μl of NuPAGE LDS sample buffer (4X) (Novex, Life Technologies) to the cell pellet. Cells were lysed by five cycles of freeze/thaw on dry ice and in a 37 °C water bath. Extracts were boiled for 5 min prior to loading. Samples were run on NuPAGE 4–12% Bis-Tris gels (Novex Life Technologies) and transferred to Invitrolon PVDF (0.45 μm pore size) membranes (Novex Life Technologies). Membranes

were incubated with affinity purified polyclonal rabbit anti-UmuC antibodies (1:7500 dilution) at room temperature overnight. Then the membranes were incubated with goat anti-rabbit IgG (H + L) alkaline phosphatase conjugate (1:10,000 dilution) (BIO-RAD). Subsequently, the membranes were treated with the CDP-Star substrate (Tropix). Membranes were then exposed to BioMax XAR film (Carestream) to visualize UmuC.

2.4. Expression and purification of pol V_{ICE391}_Y13A

Pol V_{ICE391}_Y13A was purified from RW644/ pARA1 /pJM1295 following the previously published protocol for wild-type pol V_{ICE391} [35] as a custom service by scientists at Eurofins (Dundee, United Kingdom).

2.4.1. In vitro replication assays

Wild-type *E. coli* pol V [37], wild-type pol V_{ICE391} [35], the steric gate variant pol V_{ICE391}_Y13A (this manuscript), β-clamp, and γ-complex [37] were purified as previously described. All oligonucleotides were synthesized by Lofstrand Laboratories (Gaithersburg, MD) and gel purified prior to use. The primer used for the characterization of (mis) incorporation specificity of pol V variants has the following sequences: 5A17 M (5'-GAC AAA CAA CGC GAC A). The 5′-^{32}P labeled primer was hybridized to single stranded circular M13mp18 plasmid at a 1.5:1 M ratio by heating the DNA mixtures in an annealing buffer [50 mM Tris–HCl (pH 8), 50 μg/ml BSA, 1.42 mM 2-mercaptoethanol] for 10 min at 100 °C followed by slow cooling to room temperature.

RecA (4 μM) (New England Biolabs, Ipswich, MA) was incubated with 0.25 μM 48-mer single-stranded oligonucleotide in the presence of 1 mM adenosine 5′[γ-thio]triphosphate (ATPγS, Biolog Life Science Institute, Bremen, Germany) in the 1x reaction buffer [20 mM Tris-HCl pH 7.5, 8 mM $MgCl_2$, 8 mM DTT, 80 μg/ml BSA, 4% glycerol] at 37 °C for 5 min to form RecA nucleoprotein filament on ssDNA (RecA*). Purified pol V polymerases (80 nM) were first combined with RecA* to form pol V Mut complexes [37] and then added to the reaction mixture which had been pre-incubated for 3 min at 37 °C. The reaction mixture contained 1 mM ATP, 50 μM dNTPs or rNTPs (added individually, or as a mixtures), 2 nM primed ssDNA templates (expressed as primer termini), 100 nM (as tetramer) single-stranded binding protein (SSB, Epicentre Biotechnologies, Madison, WI, USA), 50 nM (as a dimer) β-clamp and 5 nM γ-complex in the 1x reaction buffer. The reactions were incubated at 37 °C for 0.5–20 min, split into two and treated with either 0.3 M KCl, or 0.3 M KOH for 2 h at 55 °C.

For processivity measurements, primer extension reactions were carried out essentially as described above, except that the reaction mixtures contained primer-templates in sufficient excess (20-fold) over polymerase and that RecA* was pre-formed on biotinylated 48-mer oligomers (UTTA: 5′-TCG ATA CTG GTA CTA ATG ATT AAC GAC TTA AGC ACG TCC GTA CCA TCG-3′) linked to streptavidin-coated agarose resin as previously described [38]. Pol V Mut complexes were generated by incubation of wild-type pol V and pol V_{ICE391} with RecA* and isolated by centrifugation [37]. As we have shown previously [38], because pol V Mut deactivates after every round of primer extension and requires new RecA* for reactivation, addition of a trap has no effect on pol V Mut and consequently, heparin was not used in these experiments. In addition, less than 20% of the radiolabeled primer was utilized in the reactions and therefore represents replication products generated from a single polymerase-primer-template binding event [39].

All reactions were terminated by addition of an equal volume of loading buffer (97% formamide, 10 mM EDTA, 0.1% xylene cyanol, 0.1% bromophenol blue) and after heat-denaturation, the products were immediately resolved by denaturing PAGE (8 M urea, 15% acrylamide), followed by visualization using a Fuji image analyzer FLA-5100.

2.5. Measurement of leading vs. lagging strand lacZ mutagenesis

Mutant frequencies were determined for 10–30 cultures for each strain (for 2 independent *lacZ* integrants per orientation) inoculated in 2 ml LB containing 50 μg/ml spectinomycin and grown with agitation at 37 °C. After overnight incubation the appropriate dilutions of the cultures were plated on minimal-Lac plates to determine the number of Lac^+ mutants and on minimal plates containing glucose to determine the total cell count. Mutant frequencies were calculated by dividing the number of Lac^+ mutants by the total number of cells. Table 4 presents the mean values of frequencies ± 95% confidence intervals obtained from 3 independent experiments. The results for strains harboring control vector pGB2 were excluded from analyses due to negligible mutability in all tested genetic backgrounds.

Solid and liquid media were prepared as described in Fijalkowska and Schaaper [40], supplemented with appropriate amino acids and antibiotics when required.

2.6. Fluorescence microscopy

Wide-field fluorescence imaging was conducted on an inverted microscope (IX-81, Olympus with a 1.49 NA 100x objective) in an epi-fluorescence configuration [9,41]. Continuous excitation is provided using semidiode lasers (Sapphire LP, Coherent) at a wavelength of 514 nm (150 mW max. output) and 568 nm (200 mW max. output). Imaging of strains SSH118 and SSH119 were carried out on a Nikon Ti2-E microscope. Excitation light was provided by the same setup as described above. For all measurements, the sample compartment and objective lens were heated to 37 °C.

All mKate2 fusion proteins expressed from plasmids pJM1224, pJM1334, pJM1347, pJM1350 (Table 2), were imaged using yellow excitation light (λ = 568 nm) at 275 Wcm^{-2} (for colocalization measurements, imaging of RumB mutants and molecules per cell measurements), collecting emitted light between 610–680 nm (ET 645/75 m filter, Chroma) on a 512 × 512 pixel EM − CCD camera (C9100-13, Hamamatsu). For DnaX-YPet imaging, we used green excitation (λ = 514 nm) at 60 Wcm^{-2} (SSH038, SSH040, SSH073, SSH074, SSH118, SSH119), collecting light emitted between 525–555 nm (ET540/30 m filter, Chroma). Burst acquisitions in undamaged *recA730* cells (movies of 300 frames, each frame has 100 ms exposures followed by 50 ms dark time using 568 nm light) were collected to characterize the effective binding lifetimes of UmuC-mKate2 (pJM1224) and mKate2-RumB (pJM1334) as a function of foci number per cell.

Burst acquisitions (movies of 300 frames, each frame has 50 ms exposures followed by 50 ms dark time using 568 nm light) were collected to characterize the motions of UmuC and RumB fused to mKate2 (including RumB mutants), and to determine the number of UmuC-mKate2 and mKate2-RumB molecules per cell. Images of DnaX-YPet were recorded with 500 ms exposures, bright-field images were recorded with 34 ms exposures. All images were analyzed with ImageJ [42].

2.7. Flow cell designs

All imaging experiments were carried out in home-built quartz-based flow cells [9]. These flow cells were assembled from a no. 1.5 coverslip (Marienfeld, REF 0102222), a quartz top piece (45 × 20 × 1 mm) and PE-60 tubing (Instech Laboratories, Inc.). Prior to flow-cell assembly, coverslips were silanized with aminopropyltriethoxy silane (Alfa Aesar). First, coverslips were sonicated for 30 min in a 5 M KOH solution to clean and activate the surface. The cleaned coverslips were rinsed thoroughly with MilliQ water and then treated with a 5% (v/v) solution of aminopropyl-triethoxysilane (APTES) in MilliQ water. The coverslips were subsequently rinsed with ethanol and sonicated in ethanol for 20 s. Afterwards, the coverslips were rinsed with MilliQ water and dried in a jet of N_2. Silanized slides were stored under vacuum prior to use.

To assemble each flow cell, polyethylene tubing (BTPE-60, Instech

Laboratories, Inc.) was glued (BONDiT B-482, Reltek LLC) into two holes that were drilled into a quartz piece. After the glue solidified overnight, double-sided adhesive tape was adhered on two opposite sides of the quartz piece to create a channel. Then, the quartz piece was affixed to an APTES-treated coverslip. The edges were sealed with epoxy glue (5 min Epoxy, PARFIX). Each flow cell was stored in a desiccator under mild vacuum while the glue dried. Typical channel dimensions were 45 mm × 5 mm × 0.1 mm (length × width × height).

2.8. Imaging in flow cells

Cells were grown at 37 °C in EZ rich defined medium (Teknova) that contained 0.2% (wt/vol) glucose. All strains were grown in the presence of spectinomycin (50 μg/ml). Cells were loaded into flow cells, allowed a few minutes to associate with the APTES surface, then loosely associated cells were removed by pulling through fresh medium that contained spectinomycin (50 μg/ml). Throughout the experiment, medium was pulled through the flow cell using a syringe pump, at a rate of 50 μl/min.

2.9. Analysis of foci number per cell

Single cells were selected to obtain information about the number of UmuC and RumB foci present in undamaged *recA730* cells. MicrobeTracker 0.937 [43], a MATLAB script, was used to manually create cell outlines as regions of interest (ROI). By manually outlining cells, we ensure accuracy and purely select non-overlapping, in-focus cells for analysis. ImageJ 1.50i [42] was used to create average projections of effective exposure times (0.1, 7.5, 15 and 45 s). A Peak Fitter plugin, as described previously [9], was used to describe the position of each foci. The position of each defined foci was then meshed with the previously defined cell ROIs to define the number of foci per cell.

2.10. Analysis of UmuC and RumB copy numbers per cell

The number of UmuC-mKate2 and mKate2-RumB molecules and thus their concentration, are extracted from the integrated fluorescence signal under each cell outline during burst acquisition experiments. Each cell exhibits an intensity decay which is comprised of mKate2 bleaching, cellular auto-fluorescence and background fluorescence. Exciting with a laser power of 275 Wcm^{-2}, *E. coli* MG1655 cells expressing no mKate2, exhibit no auto-fluorescence. The background fluorescence was negligible (equivalent to <1 mKate2 molecule). The integrated fluorescence signal under each cell outline corresponds to the fluorescence signal of intracellular mKate2 molecules.

Images were corrected for the electronic offset and flattened to correct for inhomogeneity of the excitation beam (inhomogeneity was small at a laser power of 275 Wcm^{-2}; the brightest part at the center of the image was $<10\%$ more intense than at the corners). For each cell, the mean mKate2 signal per pixel of the first frame from the time series experiments was extracted. The mean mKate2 signal multiplied by the cell area gives the integrated mKate2 intensity, which was used to determine the number of mKate2 molecules per cell.

The mean intensity of individual mKate2 molecules was determined by analysing single-molecule return events. For each cell, the number of UmuC-mKate2 and mKate2-RumB molecules was then calculated by dividing the mean mKate2 signal of the first frame from the burst acquisition experiments by the mean single-molecule intensity. The cellular concentration was calculated using the cell volume of each cell, determined during cell outline assignation in MicrobeTracker [43].

2.11. Autocorrelation analysis

Intensity *vs.* time trajectories for UmuC-mKate2 and mKate2-RumB were extracted from fluorescence movies using ImageJ [42]. Regions of interest were defined based on the positions of DnaX-YPet foci. To capture and locally background correct mKate2 signals at these regions-of-interest, the mean intensity within a 5 × 5 pixel selection box was measured, subtracting the signal from a two-pixel ring placed around the box. This was repeated for each region-of-interest across each time-point of each movie. The resulting intensity *vs.* time trajectories, measured at each replisomal position, were imported into MATLAB. The autocorrelation function of each trajectory was calculated using the *xcorr* routine. The mean of these functions was determined for each set of data (UmuC-mKate2 or mKate2-RumB). In parallel, a mean intensity trajectory was calculated for each data set, reflecting the photobleaching kinetics. The autocorrelation function of this photobleaching curve was then calculated. To separate the effects of photobleaching from other time-dependent signal fluctuations (protein dynamics), the mean autocorrelation function for individual trajectories was divided by the autocorrelation function of the photobleaching curve. To extract time constants from the signatures detected in the normalized autocorrelation functions, the first 1 s of these signatures were fit with a single exponential decay function.

3. Results

3.1. pol V and pol V_{ICE391} dependent spontaneous mutagenesis in $dnaE^+$ and dnaE915 strains

pol V_{ICE391} is encoded by the *rumAB* genes, which were first cloned in 1993 from the IncJ plasmid, R391 [28]. Due to the fact that R391 spends much of its natural life cycle integrated into its host genome [44], it has subsequently been renamed Integrating Conjugating Element 391 (ICE391). In its native ICE environment, pol V_{ICE391} promotes minimal levels of spontaneous SOS mutagenesis [45,46]. However, when sub-cloned, pol V_{ICE391} is a potent mutator that exhibits 3–5 fold higher levels of SOS-dependent spontaneous mutagenesis compared to *E. coli* pol V [28,30]. The higher levels of mutagenesis could be due to a variety of reasons, such as higher steady-state levels of pol V_{ICE391} compared to *E. coli* pol V within the cell, or reduced fidelity during replication of undamaged DNA. Another possibility that we considered is that pol V_{ICE391} might bind to undamaged DNA more efficiently than pol V, resulting in a greater opportunity to compete with the cell's replicase, pol III. To investigate this hypothesis further, we compared the extent of pol V and pol V_{ICE391}-dependent mutagenesis in strains expressing a *dnaE915* allele. *dnaE915* (an A498T substitution in the α-catalytic subunit of the pol III replicase) was first characterized as a potential "antimutator" allele of *dnaE* [47]. It was postulated that the *dnaE915*-encoded mutant α-catalytic subunit of pol III frequently dissociates from DNA allowing any 3′-5′ exonuclease, including the intrinsic proofreading domain of DNA polymerase II, to extrinsically proofread mispaired bases at the abandoned 3′ primer terminus [48]. However, the same strains become "mutators" in the presence of SOS-induced error-prone pol V [49] which extends pol III terminal mispairs and participates more efficiently in replication after pol III dissociation. Indeed, the level of pol V-dependent SOS mutagenesis increased roughly 3-fold between $dnaE^+$ and *dnaE915* strains (Fig. 1), suggesting that pol V is not necessarily intrinsically less mutagenic than pol V_{ICE391}, but under physiological conditions, it may have limited access to undamaged genomic DNA and/or does not compete well with the wild-type α-catalytic subunit of pol III. Conversely, there was no obvious difference in the high levels of pol V_{ICE391}-dependent mutagenesis in $dnaE^+$ and *dnaE915* strains (Fig. 1), supporting the idea that pol V_{ICE391} may have better access to undamaged DNA and/or competes more efficiently with the wild-type α-catalytic subunit of pol III for access to the free 3′ primer termini, so as to promote much higher levels of spontaneous SOS mutagenesis.

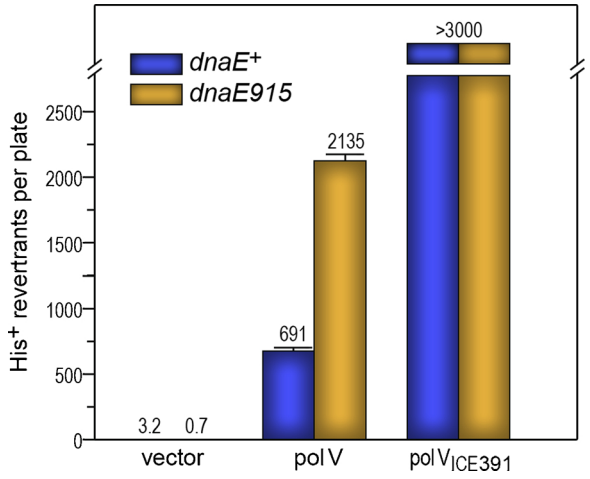

Fig. 1. Comparison of pol V- and pol V_{ICE391}-dependent spontaneous mutagenesis in *recA730 lexA51*(Def) Δ*umuDC dnaE*$^{+}$ or *dnaE915* strains. Strains were transformed with low copy plasmids pGB2 (vector); pRW134 (*umuD′C*); or pRW320 (*rumA′B*). Cultures were grown overnight in LB plus spectinomycin and processed as described in *Materials and methods* to measure reversion to histidine prototrophy. The revertants were counted after incubation at 37 °C for 4 days. The data reported represent the average number of His^{+} mutants per plate (with error bars indicating Standard Errors of the Mean [SEM]). The numbers shown above the bars are the mean values calculated from the data obtained using 3 individual cultures per strain each plated on 5 plates, for a total of 15 plates per strain.

3.2. Fluorescent protein reporters and cellular concentrations

To test the hypothesis that pol V_{ICE391} may have better access to undamaged DNA where it would compete with the cell's replisome, we used single-molecule time-lapse microscopy to directly visualize fluorescently labelled pol V and pol V_{ICE391} in live cells. We have previously used this technique to visualize the localization of a chromosomally expressed UmuC-mKate2 fusion protein [9] and have now extended these studies with plasmid encoded fluorescent constructs. So as to ensure the fusion constructs were catalytically active, we first generated low-copy number plasmids expressing UmuD′ and mKate2 fused to either the N- or C- terminus of UmuC, along with analogous RumA′ and mKate2-RumB fusions. These plasmids were introduced into *E. coli* RW584 (*recA730 lexA51*(Def) Δ*(umuDC)596::ermGT*) and the level of spontaneous mutagenesis assayed (Supplemental Fig. 1). Both N- and C-mKate2-RumB fusions were highly proficient at promoting spontaneous mutagenesis. The N-terminal fusion construct, pJM1324, promoted slightly higher levels of spontaneous mutagenesis than the untagged construct (pRW320) and was accordingly chosen for further analysis. As expected, all pol V constructs gave much lower levels of spontaneous mutagenesis than the pol V_{ICE391} constructs. The highest level of mutagenesis was observed when mKate2 was fused to the C-terminus of UmuC and as a consequence, pJM1334 was used in the fluorescence assays.

Western blots using affinity purified anti-UmuC were initially used to compare steady-state levels of the plasmid encoded untagged- and mKate2-tagged UmuC proteins (Supplemental Fig. 2). The level of UmuC-mKate2 was ~20% of that observed for wild-type UmuC. These observations are consistent with our earlier studies with chromosomally encoded *umuC*-mKate2, which also exhibited lower steady-state levels than wild-type UmuC protein [9]. The lower level of mutagenesis promoted by plasmid encoded UmuC-mKate2 compared to wild-type UmuC therefore equates to the lower steady-state levels of the fusion protein compared to the wild-type UmuC protein, rather than a change in function of the fusion protein compared to the wild-type protein.

Western blotting does not allow for ready comparison of steady-state UmuC-mKate2 and mKate2-RumB concentrations. We therefore used single-molecule fluorescence microscopy to measure these concentrations using an approach that has been described in detail previously [41]. Briefly, the integrated fluorescence intensity within each cell is measured within microscope images and normalized by the mean intensity of a single molecule, which is extracted from photobleaching traces. We found that in undamaged *recA730* cells, steady-state levels of UmuC-mKate2 were ~3-fold higher than mKate2-RumB. Specifically, cells that carried pJM1334 (UmuD′$_2$ UmuC-mKate2) contained on average 315 ± 29 molecules of UmuC-mKate2 (STD = 296; n = 80 cells), whereas cells that carried pJM1324 (RumA′$_2$ mKate2-RumB) contained 92 ± 11 molecules of mKate2-RumB (STD = 90; n = 65 cells). Taking account cell volumes, which were measured from bright-field images, these values correspond to intracellular concentrations of 40 ± 3 nM for mKate2-RumB and 101 ± 4 nM for UmuC-mKate2. Together, these results indicate that in the *recA730* background pol V_{ICE391} supports higher levels of spontaneous mutagenesis than pol V, despite its intracellular levels being lower than those of pol V. For the tagged proteins, the intracellular concentration of mKate2-RumB (40 nM) is 2.5-fold lower than for UmuC-mKate2 (101 nM).

3.3. Number and longevity of UmuC and RumB foci in undamaged recA730 cells

As the intracellular concentrations did not explain the higher levels spontaneous mutagenesis observed in pol V_{ICE391}-expressing cells, we next looked for evidence of increased polymerase activity. In single-molecule fluorescence images, we would expect individual polymerase molecules to produce foci as they bind to DNA. This phenomenon is well described and is commonly referred to as detection by localization [50]. As the polymerases bind to DNA, their diffusional motion becomes sufficiently slow that they appear as static foci in images recorded on the millisecond timescale.

To visualize fluorescently labelled pol V and pol V_{ICE391}, a bright field image was first acquired to define the position of each *recA730* Δ*umuDC* cell. Burst acquisition movies were then collected, capturing fluorescence signals from UmuC-mKate2 or mKate2-RumB signals (300 cycles of 50 ms exposure time followed by 50 ms dark time, total length of movie = 30 s). For both UmuC-mKate2 and mKate2-RumB, punctate foci were visible in most cells (Fig. 2). If foci appearing in our single-molecule images correspond to DNA polymerases actively engaged in DNA synthesis, one would predict that mutants that are defective for either DNA synthesis or impaired for substrate binding would fail to produce foci. Indeed, a catalytically inactive mutant of RumB and a mutant of RumB that is defective for binding to the β−sliding clamp, each fused to mKate2 (pJM1347 and pJM1350, respectively) failed to produce foci under conditions where the unaltered mKate2-RumB probe readily produced foci (Supplemental Fig. 3). These observations support the notion that those foci seen in the *recA730* Δ*umuDC* cells represent catalytically functional pol V, or pol V_{ICE391}.

We next set out to quantify the number of UmuC-mKate2 and mKate2-RumB foci per cell as a window into their polymerase activities. Visually comparing the UmuC-mKate2 and mKate2-RumB movies, it appeared that mKate2-RumB foci were longer-lived than the UmuC-mKate2 foci. To gain further insight into focus lifetimes, we quantified foci within average projections that captured different lengths of time. We compared the number of foci that could be detected in the first frame of the movie against projections of frames 1–3, 1–10, 1–50, 1–100, and 1–300 (Fig. 2A). This approach is equivalent to comparing images with exposure times of 0.3, 1, 5, 10 and 30 s respectively. Short effective exposure times capture both short- and long-lived foci, whereas longer effective exposure times capture long-lived foci exclusively, with short-lived foci blurring into the background. We observed similar numbers of UmuC-mKate2 and mKate2-RumB foci present in cells over all effective exposure times (Fig. 2B). For both probes approximately 2.5 foci were detected per cell in images with an effective exposure time of 0.3 s, whereas approximately 0.5 foci per cell (*i.e.* one focus per two cells) were detected in images with an effective exposure time of 30 s. It is important

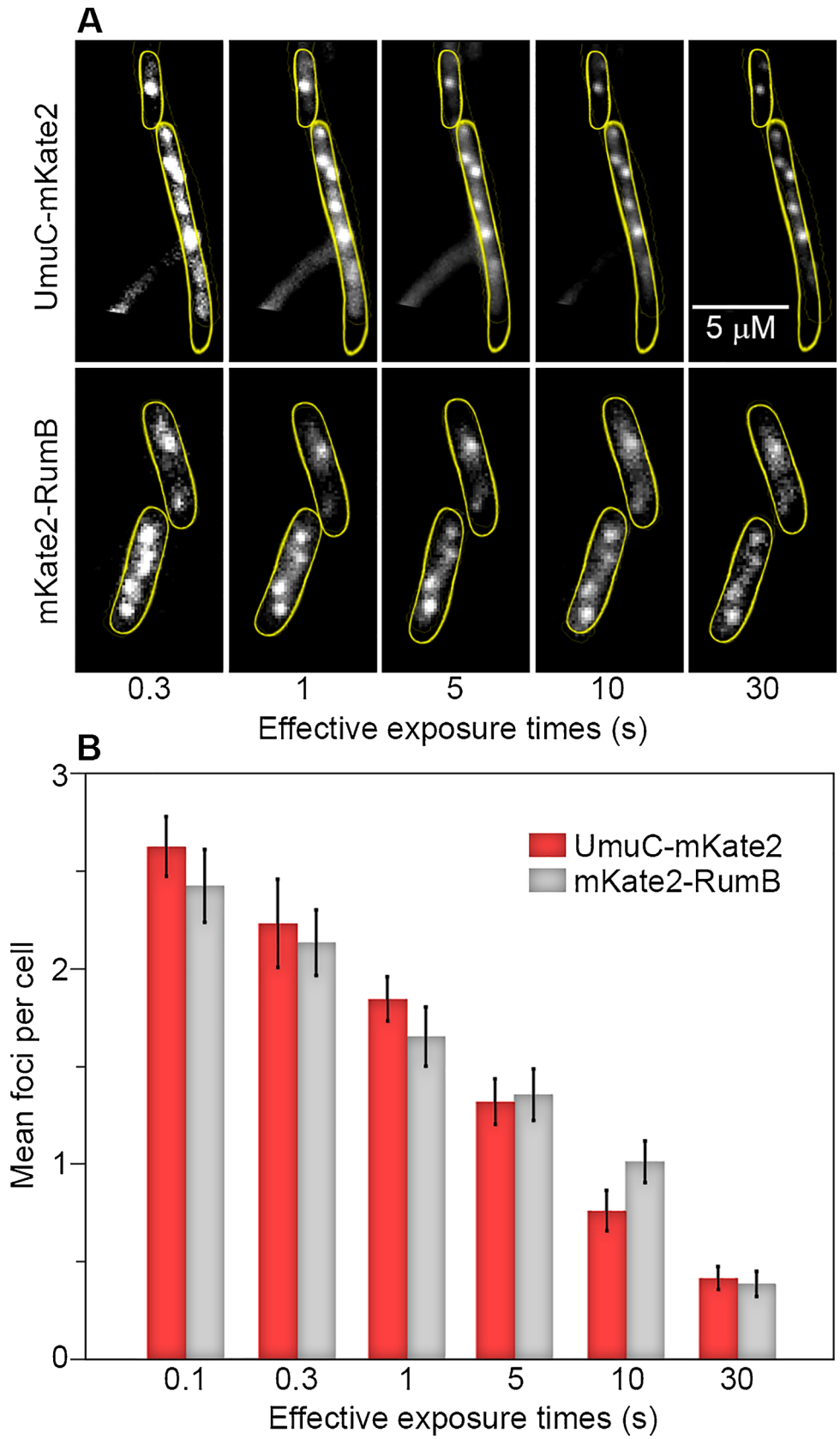

Fig. 2. Effective exposure times and number of UmuC and RumB foci in undamaged *recA730* cells. A, Top panel: Focus longevity of UmuC-mKate2 foci. Bottom panel: Focus longevity of mKate2-RumB. Scale bar 5 μm. Cells shown are representative of n > 100 cells. **B.** Mean foci per cell over longer effective exposure times. Over all projection lengths the mean number of mKate2-RumB foci per cell is similar to the mean number UmuC-mKate2 foci per cell. n > 100 cells. Error bars displayed indicate standard error of the mean.

to note that this approach does not allow for precise determination of focus lifetimes; detection of a focus in an average projection does not necessarily imply that the focus was present for the entire duration of the projection. Nevertheless, the analysis suggests that many UmuC-mKate2 and mKate2-RumB foci persist for at least a few seconds. The ratio of mKate2-RumB foci to UmuC-mKate2 foci increases with exposure time, indicating that a higher proportion of mKate2-RumB foci are longer-lived relative to the UmuC-mKate2 foci. The greater longevity of RumB foci suggests that pol V_{ICE391} may have more prolonged access to DNA than *E. coli* pol V in *recA730* cells. Interestingly, these apparent differences in focus lifetimes were much more pronounced in UV-irradiated *recA*$^+$ cells (Supplemental Fig. 4), with UmuC-mKate2 foci being rarely visible in projections longer than 10 s, whereas mKate2-RumB foci could be detected in projections of up to 80 s.

3.4. UmuC/RumB: replisome colocalization analysis in undamaged recA730 ΔumuDC cells

Having ascertained that *recA730* cells produce similar numbers of UmuC-mKate2 and mKate2-RumB foci, and that mKate2-RumB foci appear to be somewhat longer lived, we next set out to determine where the two polymerases localize within cells. Specifically, we wished to investigate whether pol V and pol V_{ICE391} differ in their colocalization with replication fork markers. To facilitate two-color imaging of pol V and pol V_{ICE391} and replisomes, the strains described above also expressed a yellow fluorescent protein fusion of the pol III HE τ-subunit (encoded by *dnaX*). We have previously used the *dnaX-YPet* fusion to indicate the position of replisomes in cells [9]. The *dnaX-YPet* allele used here is fully functional and has no impact on the growth of cells [51]. When collecting the movies described in Fig. 2, we also collected an image of the DnaX-YPet signals (500 ms exposure time) to indicate the position of replisomes.

We measured rates of colocalization between replisome markers and UmuC-mKate2/mKate2-RumB foci as a function of effective exposure time. We determined the percentage of UmuC-mKate2 foci that formed in the vicinity of replisome foci (within 218 nm [41]) and the percentage of replisome foci that contained a UmuC-mKate2 focus. Colocalization between mKate2-RumB and replisomes was determined similarly. At the shortest exposure time of 0.1 s, approximately 20% of UmuC-mKate2 foci we detected were colocalized with replisomes (Fig. 3A), in agreement with our previous measurements for chromosomally expressed UmuC-mKate2 in *recA730* cells [9]. For longer effective exposure times (0.3–30 s), the colocalization of UmuC-mKate2 foci with replisomes increased to slightly to ~30%, suggesting that longer-lived foci were more likely to form close to replisomes. Similarly, for RumB foci the colocalization increased from 25% for the shortest exposure time (0.1 s) to ~35% for longer exposure times (0.3–30 s). Thus, UmuC-mKate2 and mKate2-RumB foci colocalized with replisomes to a similar extent and exhibited similar behaviors as a function of exposure time.

The proportion of replisomes that contain a UmuC or RumB focus was also determined. Approximately 16% of replisomes had a colocalized UmuC-mKate2 focus detected at the shortest effective exposure time (Fig. 3B). Similar results were observed for mKate2-RumB. In both cases increasing the effective exposure time led to a decrease in colocalization as fewer UmuC-mKate2 or mKate2-RumB foci were detected. The increased colocalization of replisomes containing a UmuC-mKate2 focus over a group size of 30 s may be due to spurious detection of background signals as foci as a consequence of the higher steady-state levels of pol V present in the UmuC-mKate2 cells.

Overall, the results of the colocalization analysis suggest few differences between pol V and pol V_{ICE391} in *recA730* cells. Interestingly, similar

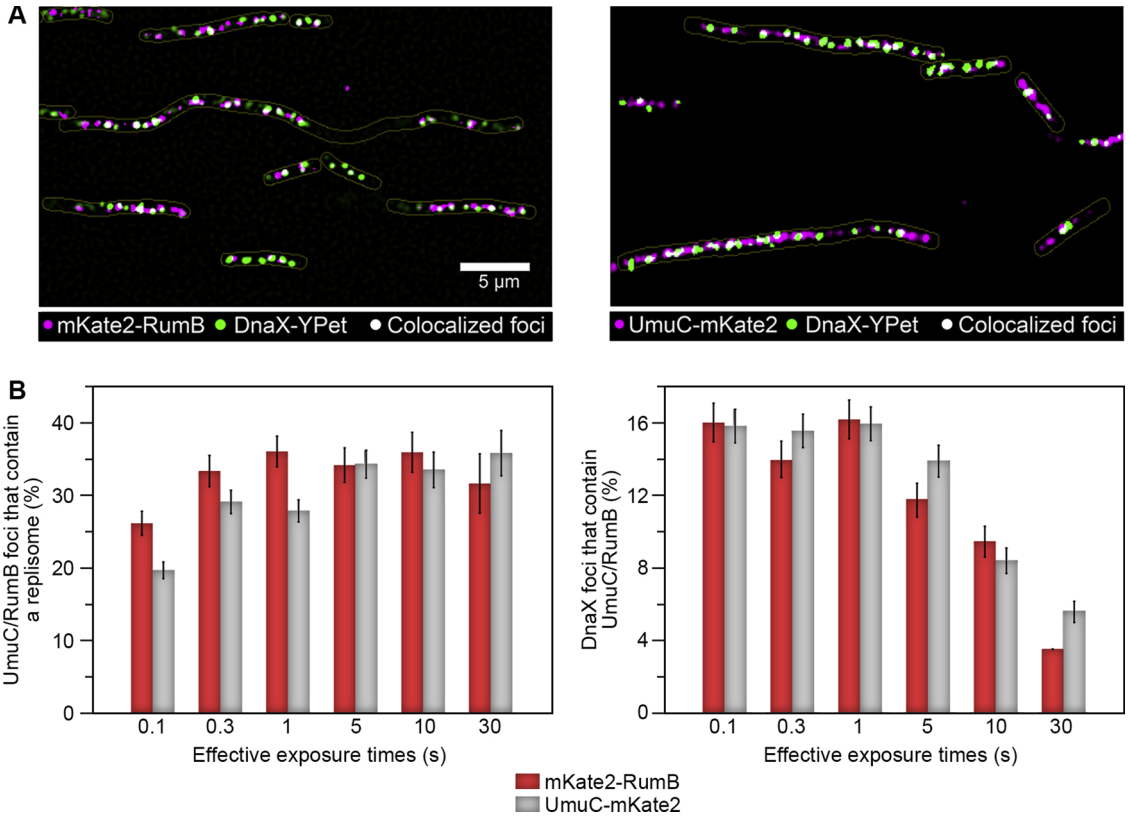

Fig. 3. Colocalization measurements of DnaX-YPet with UmuC-mKate2 or mKate2-RumB in a Δ*umuDC recA730* strain. A, Left panel: Merged images of DnaX-YPet (green) and UmuC-mKate2 (magenta, foci bound for 1 s). Right panel: Merged images of DnaX-YPet (green) and mKate2-RumB (magenta, foci bound for 1 s). Scale bar: 5 µm. **B,** Left panel: percentage of DnaX foci that contain an UmuC (grey) or RumB focus (red) at effective exposure times of 0.1, 0.3, 1, 5, 10 and 30 s. Right panel: percentage of UmuC (grey) or RumB foci (red), that overlap with DnaX foci at effective exposure times of 0.1, 0.3, 1, 5, 10 and 30 s.

analysis carried out for UV-irradiated *recA*$^+$ cells revealed stark differences between pol V and pol V_{ICE391}, with the later forming much more long-lived foci in the vicinity of replication forks (Supplemental Fig. 4). Thus, while differences in replisome colocalization and focus lifetimes can occur for pol V and pol V_{ICE391}, the two polymerases behave similarly in untreated *recA730* cells. It is therefore unlikely that the higher mutagenesis observed for pol V_{ICE391} in *recA730* cells (Fig. 1) arises as a result of increased access of pol V_{ICE391} to replication forks. Given the very high error rates of the two polymerases, frequent repetitive binding may have a major impact on the total amount of DNA synthesized by the two enzymes and thus the number of mutations they introduce, even if only a fraction of binding events lead to (mis)incorporation of nucleotides.

3.5. Repetitive binding of pol V and pol V_{ICE391} at replisomes

Thus far, the single-molecule analysis had revealed differences in pol V and pol V_{ICE391} focus lifetimes in UV-irradiated *recA*$^+$ cells but produced few clues to explain the higher rates of mutagenesis observed for pol V_{ICE391} in untreated *recA730* cells. We reasoned that pol V_{ICE391} could potentially support higher rates of mutagenesis if it simply had more robust polymerase activity than pol V once suitable substrates became available. This would allow pol V_{ICE391} to synthesize more DNA in total and therefore produce a larger number of mutations. Pursuing this idea further, we closely examined fluctuations in mKate2 fluorescence signals in regions corresponding to UmuC-mKate2 or mKate2-RumB foci. Rather than selecting regions-of-interest based on the positions of UmuC-mKate2 or mKate2-RumB foci, we monitored mKate2 signals close to replisomes, so as not to bias our results towards longer-lived (and thus more readily detected) states. Within microscope movies, intensities within 5 × 5 pixel selection boxes (large enough to capture a single focus) placed at replisomes were monitored as a function of time for both UmuC-mKate2 or mKate2-RumB in *recA730* cells.

Interestingly, the intensity *versus* time trajectories for both proteins exhibited significant evidence of dynamics occurring on the milliseconds–seconds timescale (Supplemental Fig. 5). As expected, all trajectories showed evidence of overall signal loss as a result of photobleaching, which in these measurements occurred with a time constant τ_{bleach} = 1.3 s. More strikingly, the trajectories showed frequent transitions between high and low fluorescence states, indicative of the rapid formation and loss of mKate2 foci and consistent with repeated cycles of binding and dissociation of UmuC-mKate2 and mKate2-RumB at replisome positions. Interestingly, the duration of the high fluorescence states appeared to be longer for mKate2-RumB than for UmuC-mKate2. To examine these time-dependent fluctuations more systematically, we calculated autocorrelation functions for each trajectory, comparing the mean of these functions for UmuC-mKate2 signals against mKate2-RumB signals. Repeated cycles of focus formation and loss would be expected to produce a characteristic signature in the autocorrelation functions with a lifetime that represents the combined durations of the on (high intensity, bound) and off (low intensity, unbound) states. The photobleaching-corrected autocorrelation function of UmuC-mKate2 signals produced a relatively weak signature (peaks at a value of 0.96) with a time constant τ_{acf_UmuC} = 0.05 s (Fig. 4). The equivalent autocorrelation function for mKate2-RumB signal produced a much stronger signature (peaks at a value of 0.85) with a time constant τ_{acf_RumB} = 0.35 s. The stronger signature observed for mKate2-RumB suggests that it undergoes repeated cycles of binding and dissociation at replisomes more often than UmuC-mKate2, which produces a weaker autocorrelation signature. The time constants indicate that each time mKate2-RumB binds near a replisome, it remains bound approximately seven-fold longer than UmuC-mKate2. This longer binding time may increase the likelihood that the association of the polymerase with DNA substrates would be productive (*i.e.* leading to the incorporation of nucleotides). Alternatively, longer binding could allow the polymerase to incorporate more nucleotides per binding event (*i.e.* it would have higher processivity). As these events occur repetitively, this could have a major impact on the total amount of DNA synthesized by the two enzymes and thus the number of mutations they introduce.

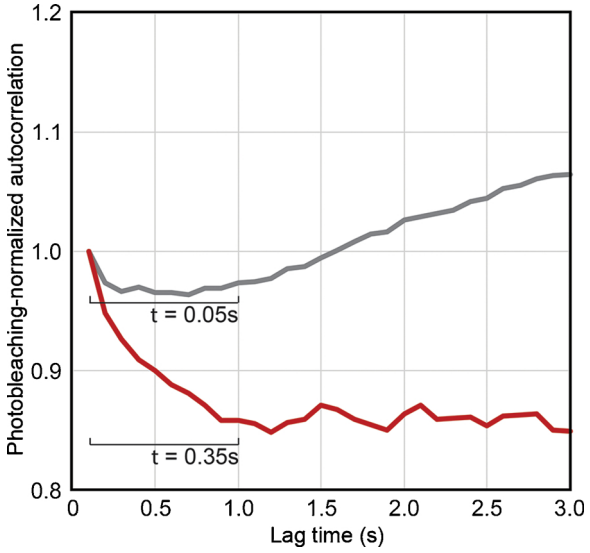

Fig. 4. Autocorrelation analysis of mKate2 signal fluctuations at replisomes. Photobleaching-normalized autocorrelation functions for UmuC-mKate2 (gray) and mKate2-RumB (red). Intensities of mKate2 signals within movies were monitored at replisome positions (Supplemental Fig. 5). Autocorrelation functions were calculated for each of the resulting intensity *vs.* time trajectories. For each data set the mean of these functions was divided by the autocorrelation function of the photobleaching curve to separate the effects of photobleaching from the effects of protein dynamics. To determine the characteristic timescale for signal fluctuations within each data set, the initial part of each autocorrelation curve (first 1 s) was fit with an exponential decay function.

3.6. Processivity of wild-type pol V and pol V_{ICE391} in vitro

We have previously characterized the biochemical properties of *E. coli* pol V and found that it shows optimal activity *in vitro* in the presence of a RecA* filament where it forms a pol V Mut complex ($UmuD'_2C$–RecA–ATP). In the presence of the β/γ-complex and single-strand DNA-binding protein (SSB) pol V Mut readily catalyzes DNA replication on circular DNA templates [37,38,52,53].

To compare the processivity of wild-type pol V and pol V_{ICE391} *in vitro* and ensure that reaction products were generated from a single polymerase-binding event, we (i) used at least 20-fold excess of primer-templates over polymerase and (ii) carried out reactions in the absence of additional RecA* (to prevent pol V Mut re-activation). However, even at the lowest enzyme-to-substrate ratios, *i.e.*, conditions that prevent re-initiation of primer extension on previously used primer-templates, the termination probabilities at most template positions changed depending on incubation time, and therefore, accurate quantification of these values is not feasible. Nevertheless, we can conclude that like pol V, pol V_{ICE391} is moderately processive (Fig. 5), generating replication products of several hundred nucleotides in length per single polymerase-binding event by ~3 min after the reaction was initiated. As seen in Fig. 5, both pol V and pol V_{ICE391} synthesized replication products with lengths gradually increasing over the 16-minute incubation period, while the overall primer utilization remained constant at all time points. The presence of strong pause sites along the DNA template, especially opposite the first ~30 bases and the fact that the length of replication products increases over at least 16 min, indicate that both polymerases, despite being moderately processive, are very slow. Indeed, we previously reported that the velocity of pol V-catalyzed DNA synthesis was ~0.3–1 nucleotides per second [37]. Under the same experimental conditions, pol V_{ICE391} appears to synthesize DNA with a faster velocity than pol V, inserting ~1.75-2 nucleotides per second (Fig. 5). As a result, pol V_{ICE391} synthesizes

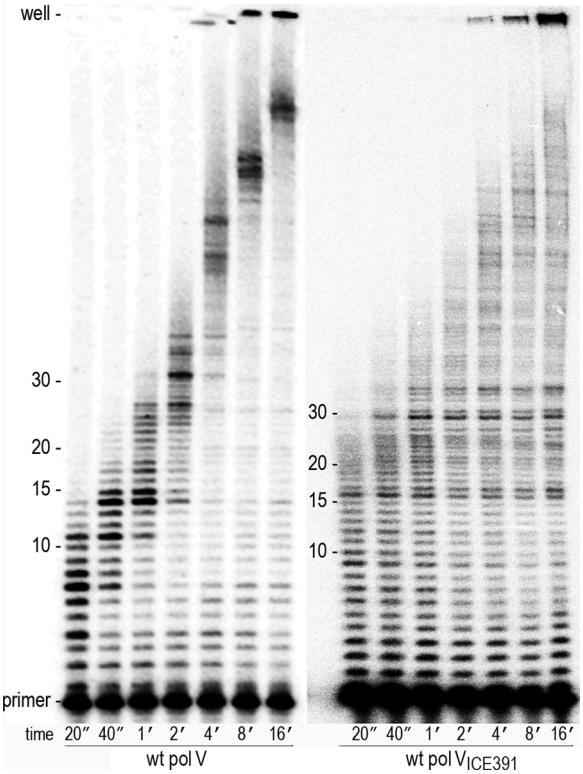

Fig. 5. Processivity and velocity of pol V and pol V_{ICE391}-catalyzed DNA synthesis. RecA was incubated for 3 min at 37 °C with biotinylated 48-mer single-stranded oligonucleotide linked to streptavidin-coated agarose resin in the presence of ATPγS to generate RecA* (RecA nucleoprotein filament). Purified wild-type pol V or pol V_{ICE391} were combined with RecA* and the resulting pol V Mut complexes were purified by centrifugation. 100 pM pol V Mut or pol V_{ICE391} Mut were added to the reaction mixtures containing 1 mM ATP, 50 μM dNTPs, 2 nM primed ssDNA templates, 100 nM SSB, 50 nM β-clamp and 5 nM γ-complex. Primer extensions were carried out at 37 °C for 20 s, 40 s, 1, 2, 4, 8, or 16 min and analyzed by PAGE. Position of the bands corresponding to the unextended primers, or primers elongated by 10–30 nucleotides, as well as the position of the wells are indicated on the left side of the gel.

substantially longer DNA products compared to pol V at the same time point. This is best seen at shorter incubation times (Fig. 5). For example, 20 s after initiation of the reactions catalyzed by pol V and pol V_{ICE391}, the primers were extended by up to ~14 and ~30 nucleotides, respectively.

3.7. Comparison of wild-type pol V_{ICE391} and pol V_{ICE391}_Y13A in vitro

Next, we compared the enzymatic properties of wild-type pol V_{ICE391} to the steric gate variant, pol V_{ICE391}_Y13A *in vitro* (Fig. 6). We have demonstrated previously that pol V exhibits an exceptional ability to misincorporate ribonucleotides into DNA *in vitro* [24]. Thus, we initially assumed that pol V_{ICE391} would discriminate against ribonucleotide incorporation as poorly as pol V. To test this hypothesis, we compared primer extension reactions in the presence of dNTPs and rNTPs (Fig. 6A, lanes 1–15). Unexpectedly, the amount and size distribution of reaction products accumulated after incubation with ATP alone, or after addition of all four NTPs, were almost identical (Fig. 6A, lanes 1–5 and 11–15). The efficiency of nucleotide incorporation and rate of the reactions with rNTPs were much lower compared to the reactions with dNTPs. For example, pol V_{ICE391} which was able to incorporate as many as 2 dNTPs every second, synthesized RNA with a rate of ~18 rNTPs per min.

We therefore conclude that pol V_{ICE391} has much more stringent sugar discrimination compared to pol V. This hypothesis can be supported by the comparison of the products of primer elongation reactions carried out in the presence of ribo- or deoxyribonucleotides with and without subsequent alkali treatment under conditions that completely hydrolyze DNA chains at the positions of rNTP insertion (Fig. 6A, lanes 4 & 5, 9 & 10, and 14 & 15). Indeed, although the reactions were carried out in the presence of ATP in 10-fold excess, pol V_{ICE391} preferred to incorporate dNTP, as judged by the negligible alkali sensitivity of reaction products (Fig. 6A, lane 10). Furthermore, products of reactions with ATP alone, or a mixture of four NTPs were only partially sensitive to alkali cleavage as judged by the presence of bands corresponding to primers elongated by 2–5 nucleotides (Fig. 6A, lanes 5, 10, and 15). These data suggest that wild-type pol V_{ICE391} discriminates against nucleotides with the wrong sugar so effectively that it prefers to incorporate dNTPs present in only miniscule amounts within the reactions (as a contaminant of NTPs).

We then determined the effect of the substitution of the steric gate residue on the *in vitro* properties of pol V_{ICE391}. The wild-type and mutant polymerases had similar overall catalytic parameters of DNA synthesis, *i.e.*, the percent of extended primers reached comparable levels for both polymerases when reactions were performed at equal enzyme/template ratios (Fig. 6A & B). However, pol V_{ICE391}_Y13A also had a distinct pattern of size distribution of replication products, *i.e.* at several positions, reaction products consisted of two bands with slightly different electrophoretic mobility (see for example doublet bands opposite the template T at the position +5, Fig. 6B, lanes 6–9). This pattern suggests that pol V_{ICE391}_Y13A catalyzes a significant degree of misincorporation opposite these sites.

As anticipated, the Y13A substitution compromised the sugar selectivity of the enzyme leading to a dramatically enhanced ability to insert rNTPs (Fig. 6B). An estimate for the time-dependent product accumulation revealed that pol V_{ICE391}_Y13A synthesized RNA with ~7 times faster rates relative to the wild-type enzyme. This is best illustrated by comparison of the products of the reactions terminated immediately after combining all ingredients (Fig. 6C, lanes labeled as "A*"). pol V_{ICE391}_Y13A promptly inserted as many as 7 AMPs, while the wild-type polymerase barely elongated primers by one ribonucleotide. DNA replication by pol V_{ICE391}_Y13A using different nucleotide substrates (NTPs and dNTPs) was not identical. For example, we detected several transient pauses specific for RNA synthesis (such as seen at positions 8 and 10). However, the velocities of DNA and RNA synthesis by pol V_{ICE391}_Y13A, length distribution of reaction products, and the maximum size of synthesized DNA and RNA were similar. In reactions where dNTPs competed with ATP present at 10-fold excess, pol V_{ICE391}_Y13A exclusively incorporated ATPs, at least opposite the first T (the first available template base). As seen in Fig. 6B, all reaction products were digested by alkali hydrolysis independently of nucleotide substrate used (lanes 5, 10, and 15).

The fidelity of the wild-type and steric gate mutant pol V_{ICE391} were compared in reactions containing each nucleotide individually (Fig. 6C). These assays suggest that both enzymes are highly error-prone and are capable of incorporating multiple wrong dNTPs. The main difference is seen in reactions performed in the presence of a single dNTP. In contrast to the wild type enzyme, pol V_{ICE391}_Y13A preferentially selects the correctly-paired ribonucleotide (ATP) rather than incorporating the correct, or incorrect dNTP. Thus, when a single dNTP was added to the reaction mixture containing pol V_{ICE391}_Y13A, ATP and DNA template with five consecutive Ts adjacent to the 3′ primer terminus, primers were extended by incorporation of at least five sequential ATPs (Fig. 6C, note similar pattern of product distribution opposite the first five template bases in all reactions with pol V_{ICE391}_Y13A).

We conclude that the major difference between wild-type pol V_{ICE391}, and the pol V_{ICE391}_Y13A mutant is the ability of the steric gate mutant to readily incorporate polyribonucleotides into DNA.

3.8. Pol V_{ICE391} _Y13A-dependent spontaneous mutagenesis

To investigate ribonucleotide incorporation by pol V_{ICE391}_Y13A in *E. coli*, we measured spontaneous His^+ mutagenesis in a *recA730 lexA*(Def)

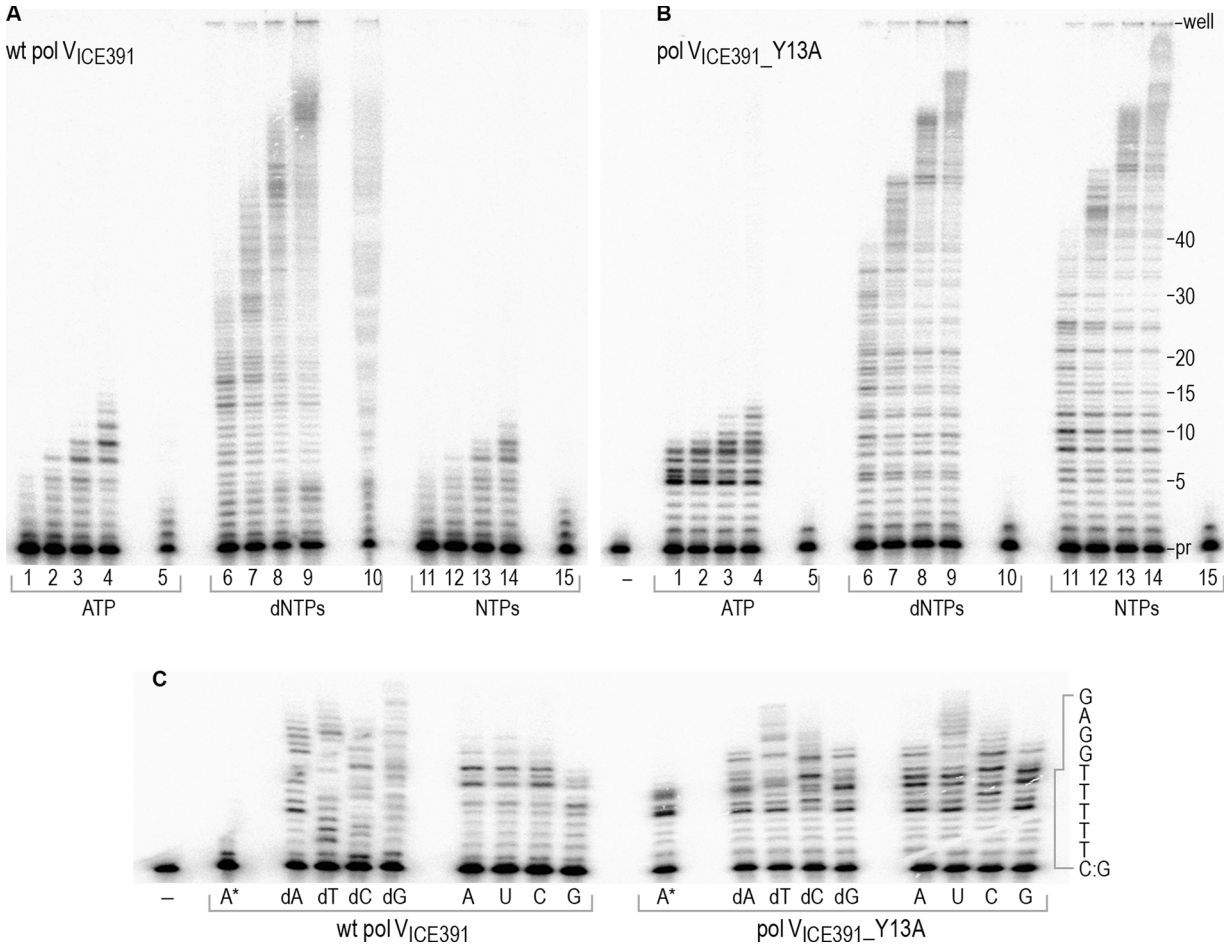

Fig. 6. Effect of a Y13A RumB substitution on the biochemical properties of pol V_{ICE391}. Primer extensions catalyzed by purified wild-type pol V_{ICE391} (**A**) and its Y13A steric gate variant (**B**) were carried out for 20 s, 1, 3, or 10 min (lanes 1–4, 6–9, 11–14 respectively) under optimal conditions. Reactions incubated for 10 min were split into two and treated with either 0.3 M KCl (lanes 4, 9, and 14) or 0.3 M KOH (lanes 5, 10, and 15) for 2 h at 55 °C. All reactions contained 1 mM ATP and were performed either in the absence of additional nucleotide (lanes 1–5, indicated as "A") or in the presence of 100 μM mixture of four dNTPs (lanes 6–10) or rNTPs (lanes 11–15). Lane with reaction mixture lacking polymerase is indicated by dash (–). Position of the bands corresponding to the unextended primers (pr) or primers elongated by 5–40 nucleotides, as well as position of the wells are indicated on the right side of the gel. (**C**). Specificity of nucleotide incorporation by wild-type pol V_{ICE391} and steric gate mutant pol V_{ICE391}_Y13A. All reactions contained 1 mM ATP. Lane with reaction lacking polymerase is indicated by dash (-) and reactions with no additional nucleotide are indicated as "A*". These reactions were terminated immediately after combining all components. Reactions in the presence of 100 μM of each nucleotide individually were carried out for 5 min. Identity of the nucleotide added to the reaction is shown below each lane. The extended sequence of templates with 5 consecutive Ts adjacent to the 3′ primer end, is indicated to the right of the gel panel. The results presented are representative of several independent experiments.

Δ*dinB* Δ*umuDC* strain. Although *recA730* is thought to be in a constitutively activated state (RecA730*), this activity can be up- or down-regulated, depending upon the genetic background of the strain [54] which leads to different levels of pol V-dependent spontaneous mutagenesis [26]. The highest level of pol V-dependent mutagenesis was observed in a Δ*rnhA* strain, which we attribute to a stronger RecA730* activating signal in this background, due to impaired replication in the absence of RNase HI, which is a pre-requisite for SOS induction. Wild-type pol V_{ICE391} exhibited high levels of spontaneous mutagenesis in all strain backgrounds. There was also an indication of the Δ*rnhA*-associated mutagenesis increase, but due to the high (>3000) number of mutants per plate, accurate quantification was unachievable (Table 3, line 3).

As observed previously with the *E. coli* pol V_Y11A mutant [26], the pol V_{ICE391}_Y13A mutant exhibited a significant (~100-fold) reduction in spontaneous mutagenesis compared to wild-type pol V_{ICE391} (Table 3, line 1). This phenotype is attributed to efficient RER targeted to misincorporated ribonucleotides, but also concomitant removal of misincorporated deoxyribonucleotides, so as to lower the overall level of spontaneous mutagenesis. In *E. coli* cells lacking RNase HII (Δ*rnhB*), pol V_{ICE391}_Y13A His^+ mutagenesis was restored from less than 1% to ~10% of wild-type pol V_{ICE391} levels (Table 3, line 2). Inactivation of RNase HI, or NER alone, had minimal effect on the level of mutagenesis promoted by pol V_{ICE391}_Y13A, which is in agreement with a lead role for RNase HII in RER (Table 3, line 2). A concomitant RNase HII-NER deficiency (Δ*rnhB* Δ*uvrA*) restored spontaneous mutagenesis to ~17% of wild-type pol V_{ICE391} (Table 3, line 4), suggesting that NER provides compensatory RER functions when RNase HII is overwhelmed, or inactivated [26]. These findings therefore support the idea that errant ribonucleotides misincorporated by pol V_{ICE391}_Y13A stimulate RER mechanisms that also result in the removal of misincorporated deoxyribonucleotides. Intriguingly, spontaneous mutagenesis promoted by pol V_{ICE391}_Y13A was not restored to the same extent as that observed for pol V_Y11A in the Δ*rnhB* or Δ*rnhB* Δ*uvrA* strains (~10% *versus* 31%, and ~17% *versus* 62%, respectively) (Table 3). We interpret these observations to indicate that RER pathways remain active, despite the loss of RNase HII and NER functions.

We assume that RNase HI is responsible for the RER. However, we could not test this hypothesis directly, since we were unable to stably introduce the pol V_{ICE391}_Y13A plasmid, pJM1282, into Δ*rnhB* Δ*rnhA*, or Δ*rnhB* Δ*rnhA* Δ*uvrA* strains when grown at either 30 °C or 37 °C. In these instances, the transformation efficiency of pJM1282 was ~1/200 of that of pRW320 (wild-type pol V_{ICE391}) and resulted in only a handful of transformants. These transformants exhibited very slow growth and

Table 3
Spontaneous mutagenesis promoted by wild type and steric gate variants of pol V and pol V_{ICE391} in *E. coli recA730 lexA*(Def) Δ*dinB* Δ*umuDC* strains.

	Status of rNMP repair genes	pGB2	pol V homologs	Wild-type polymerase	Steric Gate polymerase	SG[a] % of WT
1	wt	3.2±0.2	pol V	691±9	73±5	11
			pol V_{ICE391}	>3000	27±3	<1
2	Δ*rnhB*	2.8±0.6	pol V	671±12	207±4	31
			pol V_{ICE391}	>3000	338±6	~10
3	Δ*rnhA*	2.7±0.3	pol V	~3000	127±3	~4
			pol V_{ICE391}	≫3000	14±1	<0.5
4	Δ*uvrA*	2.9±0.6	pol V	439±2	65±1	15
			pol V_{ICE391}	>3000	44±1	~1.5
5	Δ*rnhB* Δ*uvrA*	2.9±0.4	pol V	382±14	236±15	62
			pol V_{ICE391}	>3000	503±67	~17

[a]SG: Steric gate mutant polymerase.

differing colony morphology. Furthermore, restriction digests of pJM1282 purified from the Δ*rnhB* Δ*rnhA,* or Δ*rnhB* Δ*rnhA* Δ*uvrA* strains did not match that of the parental pRW320 (Supplemental Fig. 2), suggesting increased plasmid instability under these conditions. No such instability was observed when the pol V_Y11A steric gate mutant was introduced into the Δ*rnhB* Δ*rnhA* Δ*uvrA* strain. The pJM1282 plasmid instability observed in the Δ*rnhB* Δ*rnhA,* or Δ*rnhB* Δ*rnhA* Δ*uvrA* strains is therefore directly attributed to the enhanced ability of pol V_{ICE391}_Y13A to incorporate (poly)ribonucleotides into the *E. coli* genome.

3.9. Leading vs. lagging strand mutagenesis

To test the efficiency of RER pathways on both DNA strands in strains expressing pol V_{ICE391}_Y13A, we employed a genetic system that allows us to determine the leading- and lagging- DNA strand replication fidelity [33]. The system is based on the measurement of the reversion frequency in the *lacZ* reporter gene which is integrated into the bacterial chromosome in one of two orientations with respect to the origin of replication. The target sequence is replicated as a leading strand in one orientation and as a lagging strand in the other orientation. The differences in mutant frequencies between the two orientations reflect the replication fidelity of the leading and lagging DNA strand.

It has previously been shown that differences in leading- and lagging-strand mutagenesis in certain bacterial species may be partially attributed to replication-transcription collisions occurring in cycling cells [55–57]. The concern that differential mutability of the two orientations of the reporter gene in the *E. coli lacZ* reversion system might be a consequence of replication-transcription conflicts has been addressed previously (see Discussion in [33]). In brief, the *lacZ* system was constructed so that when measuring the frequency of errors made during replication of a given DNA strand, the transcription machinery moves in the same direction (in some *lacZ* alleles) or in the opposite direction to the replication fork (in others). Thus, when differences in the fidelity of leading- and lagging-strand replication are expected, the observed *lacZ* mutation bias should always favor one DNA strand, regardless of the direction of transcription. Indeed, previous data have demonstrated that the observed mutational strand bias is not related to the orientation of the *lacZ* coding sequence (which determines the direction of transcription), but explicitly to mutations resulting from the participation and exchange during DNA leading- and lagging-strand replication by DNA polymerases [33]. Furthermore, the following studies utilizing different *lacZ* alleles in various genetic backgrounds have consistently shown that the mutation frequency on both DNA strands is not affected by the direction of transcription; in other words, despite the *lacZ* gene inversion that causes changes in the direction of transcription, the same replication fidelity strand bias has been observed [11,33,48,58–63].

Table 4
Leading- and lagging- strand mutagenesis promoted by wild type and steric gate variant of pol V_{ICE391} determined by assaying *lacZ* reversion *via* an A·T→T·A transversion.

	Status of rNMP repair genes	Strand	Frequency per10^8 cells		SG % of WT
			WT pol	SG pol	
1	wt	leading	28.9±3.9	0.8±0.3	3%
2		lagging	591.2±58.4	0.3±0.1	0.1%
3	Δ*rnhB*	leading	34.2±5.8	17.2±2.5	50%
4		lagging	575.1±55.3	4.8±0.9	0.8%
5	Δ*uvrA*	leading	22.4±2.6	1.3±0.3	6%
6		lagging	607.6±86.7	2.0±0.6	0.3%
7	Δ*rnhB* Δ*uvrA*	leading	25.2±3.4	19.9±2.8	79%
8		lagging	435.1±56.4	17.4±2.4	4%

In the current study, we assayed a *lacZ* allele that reverts *via* an A·T→T·A transversion [32], as such substitutions are the predominating pol V-dependent mutagenic events observed in a *recA730 lexA*(Def) background [64,65]. As shown in Table 4, expression of the wild-type pol V_{ICE391} from a low-copy-number plasmid in the *recA730 lexA*(Def) background resulted in a much stronger mutator effect on the lagging-strand (591.2×10^{-8}) than on the leading-strand (28.9×10^{-8}). While this observation is consistent with previously published data for wild-type pol V in a *recA730* background [11], we note that the level of mutagenesis on the lagging strand in the presence of pol V_{ICE391} is approximately 10-fold higher than that observed with pol V (unpublished observations) which again emphasizes the enhanced capacity of pol V_{ICE391} to promote SOS-dependent mutagenesis compared to pol V. In contrast, mutagenesis in the presence of the pol V_{ICE391}_Y13A mutant was notably reduced on both DNA strands, down to 3% of that observed for the wild-type on the leading- and to 0.1% on the lagging-strand. As previously proposed for the pol V_Y11A steric gate mutant [25,26], the reduction in mutagenesis is consistent with ribonucleotide-induced RER that removes misincorporated ribonucleotides, but also deoxyribonucleotides in their vicinity. The analysis of pol V_{ICE391}_Y13A-dependent mutagenesis levels in strains deficient in RNase HII and/or NER support this hypothesis. Importantly, a significant increase in mutagenesis was observed in strains lacking RNase HII (Δ*rnhB*), which is in agreement with the primary role of RNase HII-mediated RER [26]. The lack of RNase HII in strains expressing pol V_{ICE391}_Y13A significantly increases the relative mutagenesis compared to wild-type pol V_{ICE391} on the leading strand (up to 50% of that observed for the wild-type pol V_{ICE391}). The relative amount of pol V_{ICE391}_Y13A mutagenesis is also increased on the lagging strand, but only to ~1% of that of the wild-type pol V_{ICE391}. These data suggest that RNase HII plays a major role in RER on the leading strand, whereas pol V_{ICE391}_Y13A –dependent mutagenesis on the lagging strand is kept to a minimum by other ribonucleotide-directed repair pathways (*e.g.* NER, and RNase HI). Interestingly, upon inactivation of both RNase HII-dependent RER and NER, the amount of relative mutagenesis is increased to 79% on the leading- but only to 4% on the lagging- strand, suggesting that RER is still very efficient on the lagging strand, even in the absence of RNase HII and NER. We hypothesize that this is most likely due to efficient RNase HI-dependent RER that mistakes the polyribonucleotide tracts generated by pol V_{ICE391}_Y13A as primers for Okazaki fragment synthesis generated during normal genome duplication.

4. Discussion

pol V_{ICE391} is a pol V ortholog, which when sub-cloned from its native ICE391 environment, becomes a very potent, highly mutagenic DNA polymerase [29,30]. The molecular basis for the enhanced activity leading to 3–5 fold higher levels of SOS-dependent mutagenesis compared to *E. coli* pol V has been of great interest to us for over two decades [29]. Since *E. coli* pol V activity is kept to a minimum though a plethora of regulatory steps [7], it is easy to envisage that pol V_{ICE391} activity could be enhanced by its differential regulation compared to *E. coli* pol V at any of these stages. Indeed, we have recently shown that in addition to LexA-controlled transcriptional regulation, pol V_{ICE391} is subject to transcriptional control by the ICE391-encoded SetR protein [66].

Although both pol V enzymes synthesize DNA slowly (*in vitro*) and dissociate from DNA rapidly (*in vivo*), their tendency towards repetitive binding at DNA substrates and inherent low-fidelity of DNA synthesis nevertheless leads to a significant phenotypic increase in spontaneous mutagenesis *in vivo* (Fig. 1). Here, we show that the enhanced pol V_{ICE391}-dependent mutagenesis is likely due to two factors; 1) *in vitro*, pol V_{ICE391} replicates DNA ~2 to 6-fold faster than *E. coli* pol V (Fig. 6); 2) both pol V and pol V_{ICE391} bind repetitively to specific sites on the nucleoid, but with each cycle pol V_{ICE391} resides on the DNA for significantly longer than pol V (Fig. 4). Based upon these observations, low-fidelity pol V_{ICE391} would be expected to duplicate significantly more of the *E. coli* genome, which helps explain why pol V_{ICE391} promotes higher levels of mutagenesis than *E. coli* pol V, despite exhibiting a similar low-fidelity of DNA synthesis *in vitro* (c.f. Fig.1 in [24] *vs*. Fig. 6C). However, we cannot exclude the possibility of yet-to-be discovered differences in *E. coli* pol V and pol V_{ICE391} activity that may also contribute to the enhanced SOS-dependent mutator activity *in vivo*.

We have previously used a steric gate mutant of pol V to investigate the molecular mechanisms of RER in *E. coli* [25,26]. We suggested that the primary line of defense against ribonucleotides that have been incorporated by steric gate polymerase mutants is RNase HII-mediated RER, with back-up roles provided by RNase HI and NER proteins. Based upon the fact that we restored the level of spontaneous mutagenesis promoted by the pol V_Y11A mutant to that promoted by wild-type pol V, we assumed that we had identified the major participants involved in RER in *E. coli* [26]. We were therefore interested in determining if similar phenotypes might be observed with a steric gate variant of pol V_{ICE391}, which as noted above, has greater longevity in replication foci than pol V, and would therefore be expected to dramatically increase the number of errantly misincorporated ribonucleotides into the *E. coli* genome.

Similar to our earlier studies with *E. coli* pol V and a steric gate pol V_Y11A mutant [26], our *in vitro* assays indicate that both pol V_{ICE391} and pol V_{ICE391}_Y13A exhibit low fidelity DNA synthesis (Fig. 6) and both would be expected to promote high levels of spontaneous mutagenesis in a *recA730 lexA*(Def) strain if RER-functions were inactivated. Lower levels of pol V_{ICE391}_Y13A-dependent mutagenesis are therefore indicative of active RER which, during RER-patch re-synthesis, can replace incorrect deoxyribonucleotides located in the vicinity of a target ribonucleotide. Our studies using strains with deletions in *rnhB, rnhA* and *uvrA* alone, confirm that the principal pathway involved in the repair of misincorporated ribonucleotides is RNase HII-mediated RER, since there was an increase in pol V_{ICE391}_Y13A dependent mutagenesis in the Δ*rnhB* strain, but not the Δ*rnhA* or Δ*uvrA* strains (Table 3). However, the level of restoration (10% of that seen with wild-type pol V_{ICE391}) was significantly lower than observed with pol V and its steric gate mutant (Table 3). Further differences were observed in the Δ*rnhB* Δ*uvrA* strain, where pol V_{ICE391}_Y13A mutagenesis was just 17% of the wild-type pol V_{ICE391} compared to 62% for pol V_Y11A *vs*. wild-type pol V (Table 3), suggesting efficient RER, even in the absence of RNase HII, or NER proteins. The most likely candidate expected to compensate for the loss of RNase HII-dependent RER is *rnhA* encoded-RNase HI, since Δ*rnhB* strains expressing pol V_{ICE391}_Y13A and lacking *rnhA*-encoded RNase HI exhibit increased genomic/plasmid instability (Supplemental Fig. 2). This is in contrast to pol V_Y11A strains that show no-such instability even in the absence of RNase HII, RNase HI and NER proteins [26]. We therefore conclude that under circumstances where there is a significant increase in misincorporated ribonucleotides into the *E. coli* genome and the primary RNase HII-mediated RER pathway is compromised, RNase HI may play an essential role in protecting *E. coli* from the genomic instability caused by errant misincorporation of ribonucleotides. We have tacitly assumed that it reflects a simple threshold for the level of misincorporated ribonucleotides in its genome, but we cannot formally exclude the possibility that it is also the type of ribonucleotide (mono- *vs*. poly-), or the location (such as better access to the lagging strand, or at alternate origins) that leads to a greater dependency on RNase HI for genome stability in the absence of RNase HII.

Declaration of Competing Interest

The authors declare that they have no conflict of interest.

Acknowledgements

This work was supported in part, by the National Institute of Child Health and Human Development/National Institutes of Health Intramural Research Program to RW; AR was supported by Project Grant APP1165135 from the National Health and Medical Research Council; MG was supported by the National Institutes of Health grants R35ESO28343 and U19CA177547; AvO was supported by the

Australian Research Council (DP180100858 and FL140100027) National Health and Medical Research Council (APP1165135); and KMD and IF were supported by the National Science Centre, Poland, 2015/18/M/NZ3/00402.

Appendix A. Supplementary data

Supplementary material related to this article can be found, in the online version, at doi:https://doi.org/10.1016/j.dnarep.2019.102685.

References

[1] M. Tang, X. Shen, E.G. Frank, M. O'Donnell, R. Woodgate, M.F. Goodman, UmuD'$_2$C is an error-prone DNA polymerase, *Escherichia coli*, DNA pol V, Proc. Natl. Acad. Sci. U. S. A. 96 (1999) 8919–8924.

[2] H. Ohmori, E.C. Friedberg, R.P.P. Fuchs, M.F. Goodman, F. Hanaoka, D. Hinkle, T.A. Kunkel, C.W. Lawrence, Z. Livneh, T. Nohmi, L. Prakash, S. Prakash, T. Todo, G.C. Walker, Z. Wang, R. Woodgate, The Y-family of DNA polymerases, Mol. Cell 8 (2001) 7–8.

[3] T. Kato, Y. Shinoura, Isolation and characterization of mutants of *Escherichia coli* deficient in induction of mutations by ultraviolet light, Mol. Gen. Genet. 156 (1977) 121–131.

[4] G. Steinborn, Uvm mutants of *Escherichia coli* K12 deficient in UV mutagenesis. I. Isolation of *uvm* mutants and their phenotypical characterization in DNA repair and mutagenesis, Mol. Gen. Genet. 165 (1978) 87–93.

[5] R. Woodgate, Evolution of the two-step model for UV-mutagenesis, Mutat. Res. 485 (2001) 83–92.

[6] M. Jaszczur, J.G. Bertram, A. Robinson, A.M. van Oijen, R. Woodgate, M.M. Cox, M.F. Goodman, Mutations for worse or better: low-fidelity DNA synthesis by SOS DNA polymerase V is a tightly regulated double-edged sword, Biochemistry 55 (2016) 2309–2318.

[7] M.F. Goodman, J.P. McDonald, M.M. Jaszczur, R. Woodgate, Insights into the complex levels of regulation imposed on *Escherichia coli* DNA polymerase V, DNA Repair 44 (2016) 42–50.

[8] J.B. Sweasy, E.M. Witkin, N. Sinha, V. Roegner-Maniscalco, RecA protein of *Escherichia coli* has a third essential role in SOS mutator activity, J. Bacteriol. 172 (1990) 3030–3036.

[9] A. Robinson, J.P. McDonald, V.E. Caldas, M. Patel, E.A. Wood, C.M. Punter, H. Ghodke, M.M. Cox, R. Woodgate, M.F. Goodman, A.M. van Oijen, Regulation of mutagenic DNA polymerase V: activation in space and time, PLoS Genet. 11 (2015) e1005482.

[10] I.J. Fijalkowska, R.L. Dunn, R.M. Schaaper, Genetic requirements and mutational specificity of the *Escherichia coli* SOS mutator activity, J. Bacteriol. 179 (1997) 7435–7445.

[11] M. Maliszewska-Tkaczyk, P. Jonczyk, M. Bialoskorska, R.M. Schaaper, I.J. Fijalkowska, SOS mutator activity: unequal mutagenesis on leading and lagging strands, Proc. Natl. Acad. Sci. U. S. A. 97 (2000) 12678–12683.

[12] J. Neuhard, P. Nygaard, Purines and pyrimidines, in: J.L. Ingraham, K.B. Low, F.C. Neidhardt, B. Magasanik, M. Schaechter, H.E. Umbarger (Eds.), EcoSal:*Escherichia coli* and *Salmonella,* Cellular and Molecular Biology, American Society for Microbiology, Washington D.C, 1987, pp. 445–473.

[13] M.H. Buckstein, J. He, H. Rubin, Characterization of nucleotide pools as a function of physiological state in *Escherichia coli*, J. Bacteriol. 190 (2008) 718–726.

[14] P. Ferraro, E. Franzolin, G. Pontarin, P. Reichard, V. Bianchi, Quantitation of cellular deoxynucleoside triphosphates, Nucleic Acids Res. 38 (2010) e85.

[15] C.M. Joyce, Choosing the right sugar: how polymerases select a nucleotide substrate, Proc. Natl. Acad. Sci. U. S. A. 94 (1997) 1619–1622.

[16] M. Astatke, K. Ng, N.D. Grindley, C.M. Joyce, A single side chain prevents *Escherichia coli* DNA polymerase I (Klenow fragment) from incorporating ribonucleotides, Proc. Natl. Acad. Sci. U. S. A. 95 (1998) 3402–3407.

[17] A. Vaisman, R. Woodgate, Redundancy in ribonucleotide excision repair: competition, compensation, and cooperation, DNA Repair 29 (2015) 74–82.

[18] S.A. Nick McElhinny, D. Kumar, A.B. Clark, D.L. Watt, B.E. Watts, E.B. Lundstrom, E. Johansson, A. Chabes, T.A. Kunkel, Genome instability due to ribonucleotide incorporation into DNA, Nat. Chem. Biol. 6 (2010) 774–781.

[19] S.A. Nick McElhinny, B.E. Watts, D. Kumar, D.L. Watt, E.B. Lundstrom, P.M. Burgers, E. Johansson, A. Chabes, T.A. Kunkel, Abundant ribonucleotide incorporation into DNA by yeast replicative polymerases, Proc. Natl. Acad. Sci. U. S. A. 107 (2010) 4949–4954.

[20] F. Lazzaro, D. Novarina, F. Amara, D.L. Watt, J.E. Stone, V. Costanzo, P.M. Burgers, T.A. Kunkel, P. Plevani, M. Muzi-Falconi, RNase H and postreplication repair protect cells from ribonucleotides incorporated in DNA, Mol. Cell 45 (2012) 99–110.

[21] J.L. Sparks, H. Chon, S.M. Cerritelli, T.A. Kunkel, E. Johansson, R.J. Crouch, P.M. Burgers, RNase H2-Initiated ribonucleotide excision repair, Mol. Cell 47 (2012) 980–986.

[22] J.S. Williams, D.B. Gehle, T.A. Kunkel, The role of RNase H2 in processing ribonucleotides incorporated during DNA replication, DNA Repair 53 (2017) 52–58.

[23] A. Vaisman, R. Woodgate, Ribonucleotide discrimination by translesion synthesis DNA polymerases, Crit. Rev. Biochem. Mol. Biol. 53 (2018) 382–402.

[24] A. Vaisman, W. Kuban, J.P. McDonald, K. Karata, W. Yang, M.F. Goodman, R. Woodgate, Critical amino acids in *Escherichia coli* responsible for sugar discrimination and base-substitution fidelity, Nucleic Acids Res. 40 (2012) 6144–6157.

[25] J.P. McDonald, A. Vaisman, W. Kuban, M.F. Goodman, R. Woodgate, Mechanisms employed by *Escherichia coli* to prevent ribonucleotide incorporation into genomic DNA by pol V, PLoS Genet. 8 (2012) e1003030.

[26] A. Vaisman, J.P. McDonald, D. Huston, W. Kuban, L. Liu, B. Van Houten, R. Woodgate, Removal of misincorporated ribonucleotides from prokaryotic genomes: an unexpected role for nucleotide excision repair, PLoS Genet. 9 (2013) e1003878.

[27] J.C. McCann, N.E. Springarn, J. Kobari, B.N. Ames, Detection of carcinogens as mutagens: bacterial tester strains with R factor plasmids, Proc. Natl. Acad. Sci. U. S. A. 72 (1975) 979–983.

[28] C. Ho, O.I. Kulaeva, A.S. Levine, R. Woodgate, A rapid method for cloning mutagenic DNA repair genes: isolation of *umu*-complementing genes from multidrug resistance plasmids R391, R446b, and R471a, J. Bacteriol. 175 (1993) 5411–5419.

[29] O.I. Kulaeva, J.C. Wootton, A.S. Levine, R. Woodgate, Characterization of the *umu*-complementing operon from R391, J. Bacteriol. 177 (1995) 2737–2743.

[30] S. Mead, A. Vaisman, M. Valjavec-Gratian, K. Karata, D. Vandewiele, R. Woodgate, Characterization of polV$_{R391}$: a Y-family polymerase encoded by *rumA'B* from the IncJ conjugative transposon, R391, Mol. Microbiol. 63 (2007) 797–810.

[31] J.H. Miller, A Short Course in Bacterial Genetics: A Laboratory Manual and Handbook for *Escherichia coli* and Related Bacteria, Cold Spring Harbor Laboratory Press, Cold Spring Harbor, N.Y, 1992.

[32] C.G. Cupples, J.H. Miller, A set of *lacZ* mutations in *Escherichia coli* that allow rapid detection of each of the six base substitutions, Proc. Natl. Acad. Sci. U. S. A. 86 (1989) 5345–5349.

[33] I.J. Fijalkowska, P. Jonczyk, M.M. Tkaczyk, M. Bialoskorska, R.M. Schaaper, Unequal fidelity of leading strand and lagging strand DNA replication on the *Escherichia coli* chromosome, Proc. Natl. Acad. Sci. U. S. A. 95 (1998) 10020–10025.

[34] E.S.J. Szekeres, R. Woodgate, C.W. Lawrence, Substitution of *mucAB* or *rumAB* for *umuDC* alters the relative frequencies of the two classes of mutations induced by a site-specific T-T cyclobutane dimer and the efficiency of translesion DNA synthesis, J. Bacteriol. 178 (1996) 2559–2563.

[35] A.J. Gruber, A.L. Erdem, G. Sabat, K. Karata, M.M. Jaszczur, D.D. Vo, T.M. Olsen, R. Woodgate, M.F. Goodman, M.M. Cox, A RecA protein surface required for activation of DNA polymerase V, PLoS Genet. 11 (2015) e1005066.

[36] B.D. Davis, E.S. Mingioli, Mutants of *Escherichia coli* requiring methionine or vitamin B12, J. Bacteriol. 60 (1950) 17–28.

[37] K. Karata, A. Vaisman, M.F. Goodman, R. Woodgate, Simple and efficient purification of *Escherichia coli* DNA polymerase V: cofactor requirements for optimal activity and processivity *in vitro*, DNA Repair 11 (2012) 431–440.

[38] Q. Jiang, K. Karata, R. Woodgate, M.M. Cox, M.F. Goodman, The active form of DNA polymerase V is UmuD'$_2$C-RecA-ATP, Nature 460 (2009) 359–363.

[39] M.S. Boosalis, J. Petruska, M.F. Goodman, DNA polymerase insertion fidelity. Gel assay for site-specific kinetics, J. Biol. Chem. 262 (1987) 14689–14696.

[40] I.J. Fijalkowska, R.M. Schaaper, Effects of *Escherichia coli dnaE* antimutator alleles in a proofreading- deficient *mutD5* strain, J. Bacteriol. 177 (1995) 5979–5986.

[41] S.S. Henrikus, E.A. Wood, J.P. McDonald, M.M. Cox, R. Woodgate, M.F. Goodman, A.M. van Oijen, A. Robinson, DNA polymerase IV primarily operates outside of DNA replication forks in *Escherichia coli*, PLoS Genet. 14 (2018) e1007161.

[42] C.A. Schneider, W.S. Rasband, K.W. Eliceiri, NIH Image to ImageJ: 25 years of image analysis, Nat. Methods 9 (2012) 671–675.

[43] O. Sliusarenko, J. Heinritz, T. Emonet, C. Jacobs-Wagner, High-throughput, subpixel precision analysis of bacterial morphogenesis and intracellular spatio-temporal dynamics, Mol. Microbiol. 80 (2011) 612–627.

[44] R.A. Wozniak, D.E. Fouts, M. Spagnoletti, M.M. Colombo, D. Ceccarelli, G. Garriss, C. Dery, V. Burrus, M.K. Waldor, Comparative ICE genomics: insights into the evolution of the SXT/R391 family of ICEs, PLoS Genet. 5 (2009) e1000786.

[45] R.J. Pinney, Distribution among incompatibility groups of plasmids that confer UV mutability and UV resistance, Mutat. Res. 72 (1980) 155–159.

[46] C. Upton, R.J. Pinney, Expression of eight unrelated Muc$^+$ plasmids in eleven DNA repair-deficient *E. coli* strains, Mutat. Res. 112 (1983) 261–273.

[47] I.J. Fijalkowska, R.M. Schaaper, Antimutator mutations in the a subunit of *Escherichia coli* DNA polymerase III: identification of the responsible mutations and alignment with other DNA polymerases, Genetics 134 (1993) 1039–1044.

[48] M. Banach-Orlowska, I.J. Fijalkowska, R.M. Schaaper, P. Jonczyk, DNA polymerase II as a fidelity factor in chromosomal DNA synthesis in *Escherichia coli*, Mol. Microbiol. 58 (2005) 61–70.

[49] K.H. Maslowska, K. Makiela-Dzbenska, J.Y. Mo, I.J. Fijalkowska, R.M. Schaaper, High-accuracy lagging-strand DNA replication mediated by DNA polymerase dissociation, Proc. Natl. Acad. Sci. U. S. A. 115 (2018) 4212–4217.

[50] J. Elf, G.W. Li, X.S. Xie, Probing transcription factor dynamics at the single-molecule level in a living cell, Science 316 (2007) 1191–1194.

[51] J.S. Lewis, L.M. Spenkelink, S. Jergic, E.A. Wood, E. Monachino, N.P. Horan, K.E. Duderstadt, M.M. Cox, A. Robinson, N.E. Dixon, A.M. van Oijen, Single-molecule visualization of fast polymerase turnover in the bacterial replisome, Elife 6 (2017).

[52] K. Schlacher, K. Leslie, C. Wyman, R. Woodgate, M.M. Cox, M.F. Goodman, DNA polymerase V and RecA protein, a minimal mutasome, Mol. Cell 17 (2005) 561–572.

[53] K. Schlacher, M.M. Cox, R. Woodgate, M.F. Goodman, RecA acts in trans to allow replication of damaged DNA by DNA polymerase V, Nature 442 (2006) 883–887.

[54] I. Vlašić, A. Šimatović, K. Brčić-Kostić, Genetic requirements for high constitutive SOS expression in *recA730* mutants of *Escherichia coli*, J. Bacteriol. 193 (2011) 4643–4651.

[55] S. Paul, S. Million-Weaver, S. Chattopadhyay, E. Sokurenko, H. Merrikh, Accelerated gene evolution through replication-transcription conflicts, Nature 495 (2013) 512–515.

[56] S. Million-Weaver, A.N. Samadpour, D.A. Moreno-Habel, P. Nugent, M.J. Brittnacher, E. Weiss, H.S. Hayden, S.I. Miller, I. Liachko, H. Merrikh, An underlying mechanism for the increased mutagenesis of lagging-strand genes in *Bacillus subtilis*, Proc. Natl. Acad. Sci. U. S. A. 112 (2015) E1096–1105.
[57] T.S. Sankar, B.D. Wastuwidyaningtyas, Y. Dong, S.A. Lewis, J.D. Wang, The nature of mutations induced by replication-transcription collisions, Nature 535 (2016) 178–181.
[58] D. Gawel, M. Maliszewska-Tkaczyk, P. Jonczyk, R.M. Schaaper, I.J. Fijalkowska, Lack of strand bias in UV-induced mutagenesis in *Escherichia coli*, J. Bacteriol. 184 (2002) 4449–4454.
[59] D. Gawel, P. Jonczyk, I.J. Fijalkowska, R.M. Schaaper, dnaX36 Mutator of *Escherichia coli*: effects of the τ subunit of the DNA polymerase III holoenzyme on chromosomal DNA replication fidelity, J. Bacteriol. 193 (2011) 296–300.
[60] D. Gawel, I.J. Fijalkowska, P. Jonczyk, R.M. Schaaper, Effect of dNTP pool alterations on fidelity of leading and lagging strand DNA replication in *E. coli*, Mutat. Res. 759 (2014) 22–28.
[61] W. Kuban, P. Jonczyk, D. Gawel, K. Malanowska, R.M. Schaaper, I.J. Fijalkowska, Role of *Escherichia coli* DNA polymerase IV in *in vivo* replication fidelity, J. Bacteriol. 186 (2004) 4802–4807.
[62] W. Kuban, M. Banach-Orlowska, M. Bialoskorska, A. Lipowska, R.M. Schaaper, P. Jonczyk, I.J. Fijalkowska, Mutator phenotype resulting from DNA polymerase IV overproduction in *Escherichia coli*: preferential mutagenesis on the lagging strand, J. Bacteriol. 187 (2005) 6862–6866.
[63] K. Makiela-Dzbenska, M. Jaszczur, M. Banach-Orlowska, P. Jonczyk, R.M. Schaaper, I.J. Fijalkowska, Role of *Escherichia coli* DNA polymerase I in chromosomal DNA replication fidelity, Mol. Microbiol. 74 (2009) 1114–1127.
[64] M. Watanabe-Akanuma, R. Woodgate, T. Ohta, Enhanced generation of A:T→T:A transversions in a *recA730 lexA51*(Def) mutant of *Escherichia coli*, Mutat. Res. 373 (1997) 61–66.
[65] E. Curti, J.P. McDonald, S. Mead, R. Woodgate, DNA polymerase switching: effects on spontaneous mutagenesis in *Escherichia coli*, Mol. Microbiol. 71 (2009) 315–331.
[66] M. Gonzalez, D. Huston, M.P. McLenigan, J.P. McDonald, A.M. Garcia, K.S. Borden, R. Woodgate, $SetR_{ICE391}$, a negative transcriptional regulator of the integrating conjugative element 391 mutagenic response, DNA Repair 73 (2019) 99–109.
[67] G. Lia, B. Michel, J.F. Allemand, Polymerase exchange during Okazaki fragment synthesis observed in living cells, Science 335 (2012) 328–331.
[68] R. Woodgate, Construction of a *umuDC* operon substitution mutation in *Escherichia coli*, Mutat. Res. 281 (1992) 221–225.
[69] D. Vandewiele, A.R. Fernández de Henestrosa, A.R. Timms, B.A. Bridges, R. Woodgate, Sequence analysis and phenotypes of five temperature sensitive mutator alleles of *dnaE*, encoding modified α-catalytic subunits of *Escherichia coli* DNA polymerase III holoenzyme, Mutat. Res. 499 (2002) 85–95.
[70] R.M. Schaaper, The mutational specificity of two *Escherichia coli dnaE* antimutator alleles as determined from *lacI* mutation spectra, Genetics 134 (1993) 1031–1038.
[71] G. Churchward, D. Belin, Y. Nagamine, A pSC101-derived plasmid which shows no sequence homology to other commonly used cloning vectors, Gene 31 (1984) 165–171.
[72] W. Kuban, A. Vaisman, J.P. McDonald, K. Karata, W. Yang, M.F. Goodman, R. Woodgate, *Escherichia coli* UmuC active site mutants: effects on translesion DNA synthesis, mutagenesis and cell survival, DNA Repair 11 (2012) 726–732.